

Fine Tuning the Performance of DSSCs by Variation of the π -Spacers in Organic Dyes that Contain a 2,7-Diaminofluorene Donor

Abhishek Baheti,^[a] K. R. Justin Thomas,^{*[a]} Chuan-Pei Lee,^[b] and Kuo-Chuan Ho^[b]

Abstract: Organic dyes that contain a 2,7-diaminofluorene-based donor, a cyanoacrylic-acid acceptor, and various aromatic conjugation segments, which are composed of benzene, fluorene, carbazole, and thiophene units, as a π -bridge have been synthesized and characterized by optical, electrochemical, and theoretical investigations. The trends in the absorption and electrochemical properties of these dyes are in accordance with the electron-donating ability of the conjugating segment.

Consequently, the dyes that contained a 2,7-carbazole unit in the π -spacer exhibited red-shifted absorption and lower oxidation potentials than their corresponding fluorene- and phenylene-bridged dyes. However, the enhanced power-conversion efficiency

Keywords: density functional calculations • donor–acceptor systems • dyes/pigments • fluorene • solar cells

that was exhibited by the fluorene-bridged dyes in the DSSCs was attributed to their broader and intense absorption. Despite the longer-wavelength absorption and reasonable optical density, carbazole-bridged dyes exhibited lower power-conversion efficiencies, which were ascribed to the poor alignment of the LUMO level in these dyes, thereby leading to the inhibition of electron injection into the TiO₂ conduction band.

Introduction

Metal-free organic dyes^[1] are considered to be a fascinating choice for the conversion of solar energy into electricity by using photoelectrochemical cells, despite the superior performance of ruthenium-based dyes.^[2] Ruthenium dyes suffer from disadvantages such as high cost, lower molar extinction coefficients, and the need for tedious purification steps in their synthesis.^[2] On the other hand, organic dyes are cheap, they display larger molar absorption coefficients, and their chemical modification can be performed by using simple methods.^[1] Most of the currently used organic sensitizers are constructed from several structural elements, such as a donor (D) and an acceptor (A) that are bridged by a suitable π -conjugation unit (D– π –A).^[1] Apart from this standard arrangement, in recent years, a number of dyes that featured other structural formats, such as D– π –D–A,^[3] D–D– π –A,^[4] and D–A– π –A,^[5] have also been explored in an attempt to improve the power-conversion efficiency of their corresponding dye-sensitized solar cells (DSSCs). It has been

found that two factors significantly contribute to a drop in device efficiency: 1) the formation of dye aggregates and 2) charge recombination between the conduction-band electrons and the oxidized dye or electrolyte. Aggregation at the TiO₂ surface can be hindered by introducing lateral alkyl chains or other hindering units.^[6] The minimization of “dark current” may be achieved by suitably adjusting the energies of the dyes and electrolytes.^[7] To evolve these methods so as to minimize the influence of these factors, systematic structure–property relationship studies are necessary on dyes that show promising performance in DSSCs.

Organic dyes that contain triarylamine donors and cyanoacrylic-acid acceptors that are bridged by various aromatic segments, such as oligothiophenes,^[8] benzothiadiazoles,^[9] benzotriazoles,^[10] etc., have been developed as promising sensitizers for DSSCs. It has been generally noted that the incorporation of triarylamines that contain electron-rich units, such as fluorenes^[11] and alkoxy-substituted benzenes,^[12] is beneficial for realizing favorable electronic properties. We have recently found that the introduction of auxiliary donors onto fluorene-based triarylamines helped to improve the optical, electrochemical, and photovoltaic properties of their corresponding dyes.^[13] It has also been generally accepted that a change in the nature of the conjugation pathway that bridges the donor and acceptor fragments in the organic dyes is an effective way to fine tune the electronic properties of the dyes.^[1] There is ample evidence in the literature on the involvement of bridging units in charge-separation kinetics.^[1] Although the coplanar π -conjugating segment is beneficial for red-shifting the absorption wavelength, non-coplanar bridges have enhanced the probabilities of charge separation and charge injection.^[14] In addi-

[a] A. Baheti, Dr. K. R. J. Thomas
Organic Materials Laboratory, Department of Chemistry
Indian Institute of Technology Roorkee
Roorkee–247 667 (India)
Fax: (+91) 1332-286202
E-mail: krjt8fcy@iitr.ernet.in

[b] C.-P. Lee, Prof. Dr. K.-C. Ho
Department of Chemical Engineering
National Taiwan University
Taipei 10617 (Taiwan)

Supporting information for this article is available on the WWW under <http://dx.doi.org/10.1002/asia.201200752>.

tion, the introduction of an energy-delocalizing chromophore into the conjugation pathway may cause prolongation of the excited state and, eventually, could favor electron ejection. Herein, we have varied the conjugation bridge between the donor and the acceptor, by incorporating phenyl/fluorene/carbazole and thiophene units, thereby developing six new dyes. As an electron-rich unit, fluorene and carbazole may improve the redox stability of the dyes and their dye-regeneration propensities. Carbazole is commonly used as a donor because of its good thermal, electrochemical stability, and hole-transporting properties.^[15] We used a 2,7-disubstituted carbazole in the bridge on the assumption that it would effectively enhance the conjugation and serve as effective charge-delocalizing segment in comparison to the

3,6-disubstituted carbazole. The newly developed dyes showed significant enhancement in terms of their optical and electrochemical properties when compared to their analogous derivatives that contained a simple phenylene spacer^[13] between the donor and acceptor and, consequently, served as efficient sensitizers in DSSCs (see above).

Results and Discussion

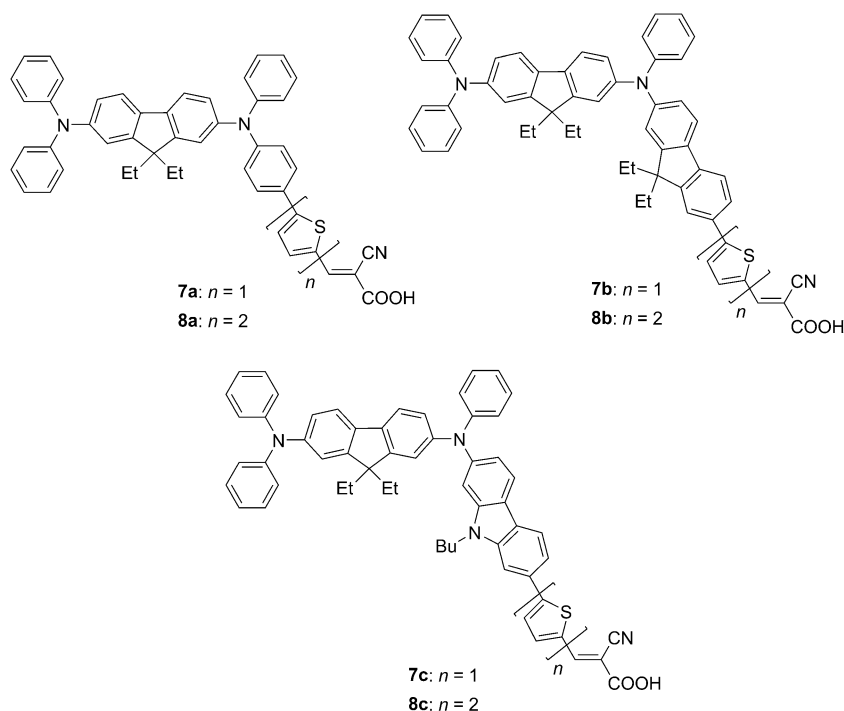
Synthesis and Characterization

The synthetic pathways that lead to the formation of the targeted dyes are shown in Scheme 1. Fluorenediamine-based aryl bromides *N*²-(4-bromophenyl)-9,9-diethyl-*N*²,*N*⁷,*N*⁷-triphenyl-9*H*-fluorene-2,7-diamine (**4a**), *N*²-(7-bromo-9,9-diethyl-9*H*-fluorene-2-yl)-9,9-diethyl-*N*²,*N*⁷,*N*⁷-triphenyl-9*H*-fluorene-2,7-diamine (**4b**), and *N*²-(7-bromo-9-butyl-9*H*-carbazol-2-yl)-9,9-diethyl-*N*²,*N*⁷,*N*⁷-triphenyl-9*H*-fluorene-2,7-diamine (**4c**) were either synthesized from 9,9-diethyl-*N*²,*N*²,*N*⁷,*N*⁷-tetraphenyl-9*H*-fluorene-2,7-diamine (**3**)^[16] in a single-step bromination reaction or from 7-bromo-9,9-diethyl-*N,N*-diphenyl-9*H*-fluorene-2-amine (**1**) in two steps that involved consecutive Pd-catalyzed C–N coupling reactions^[17] with aniline and 2,7-dibromo-9,9-diethyl-9*H*-fluorene or 2,7-dibromo-9-butyl-9*H*-carbazole. These compounds were then converted into their corresponding substituted thienyl aldehydes (**5** and **6**) through Stille coupling reactions^[18] and

subsequent acid hydrolysis (Scheme 1). Finally, the aldehydes were converted into their desired cyanoacrylic-acid derivatives (**7** and **8**) through Knoevenagel condensation.^[19] The dyes were thoroughly characterized by ¹H and ¹³C NMR spectroscopy and by MS. These dyes were dark red in color and were reasonably soluble in common solvents, such as toluene, tetrahydrofuran (THF), EtOAc, CH₂Cl₂, MeCN, etc.

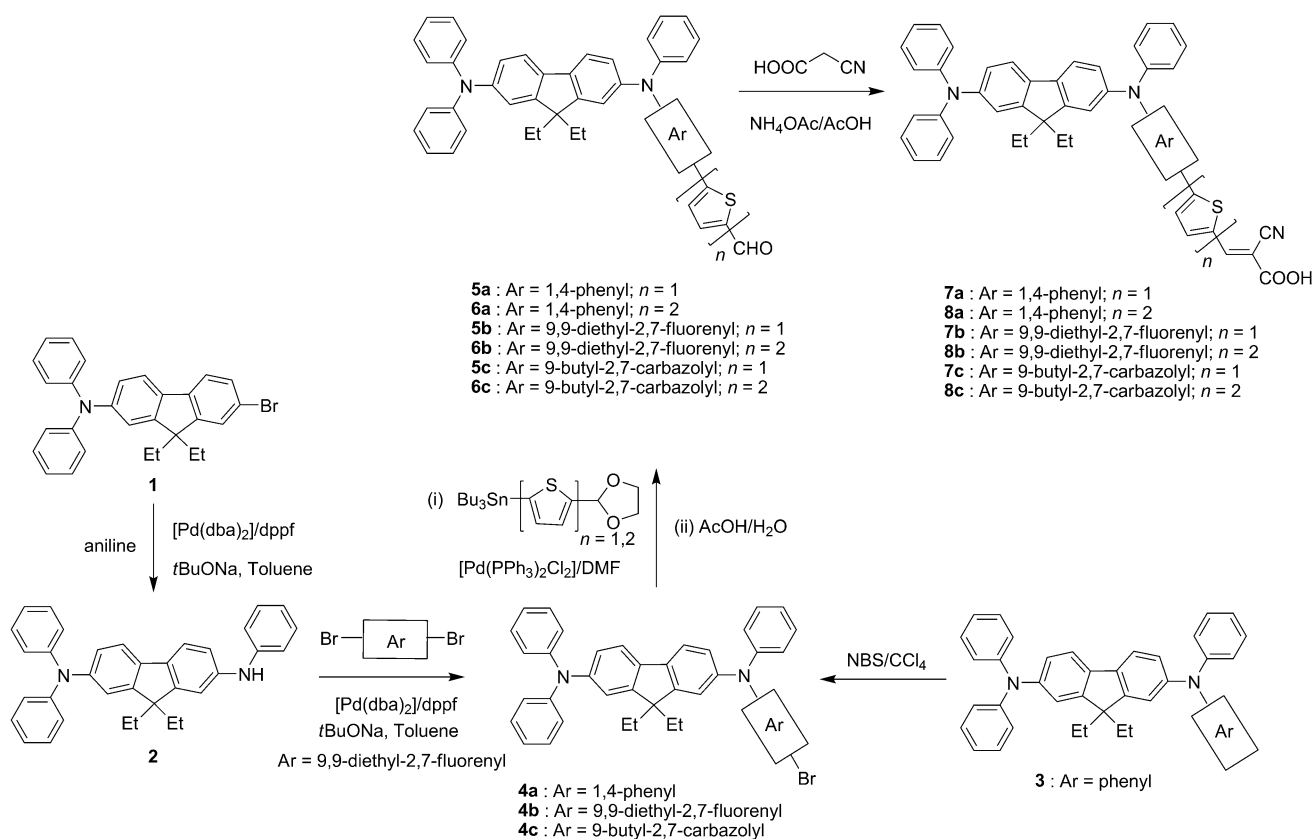
Photophysical Properties

The absorption spectra of the dyes in CH₂Cl₂ are presented in Figure 1. All of the dyes exhibit two prominent absorption peaks in the regions 374–384 nm and 487–506 nm (Table 1). The peaks at shorter wavelengths (<400) are assigned to localized π–π* transitions that originate from the diphenylamine, aminofluorene, and π-linker segments, whilst the peaks at longer wavelengths (>485 nm) are at-



Abstract in Hindi:

बेंजिन, फ्लुओरीन, कार्बाजोल और थायोफीन युक्त पाई ब्रिज वाले कार्बनिक रन्जक जिनमें 2,7-डाईएमीनोफ्लुओरीन दाता एंव सायनोएसिटिक अम्ल ग्राही है का संश्लेषण तथा उनका आप्टिकल, विद्युत और सैद्धान्तिक विश्लेषण किया गया है। इनके द्वारा रंगों कि अवशोषण क्षमता एवम् विद्युत गुण योजक खंडों कि इलेक्ट्रान दान करने कि क्षमता के अनुसार है। नतीजतन 2,7-कार्बाजोल युक्त इकाई फ्लुओरीन तथा बेंजिन की तुलना मे लाल रंग की ओर अधिक अवशोषण एवम् कम आक्सिकरण क्षमता दिखाती है। हालांकि फ्लुओरीन आधारित डी एस एस सी कि अधिक उर्जा परिवर्तन क्षमता के लिए इसकी व्यापक तथा गहन अवशोषण क्षमता को जिम्मेदार माना गया है। यद्यपि कार्बाजोल युक्त रन्जक थंखला तरन्दाधैर्य अवशोषण एवम् आप्टिकल घनत्व के हिसाब से उचित है परन्तु इसकी कम उर्जा परिवर्तन क्षमता का कारण इसके लूमो के टाइटेनियम डाई ऑक्साइड के प्रवाहकत्व बैंड के साथ अल्प संरेखण को माना गया है।



Scheme 1. Synthesis of dyes **7** and **8**.

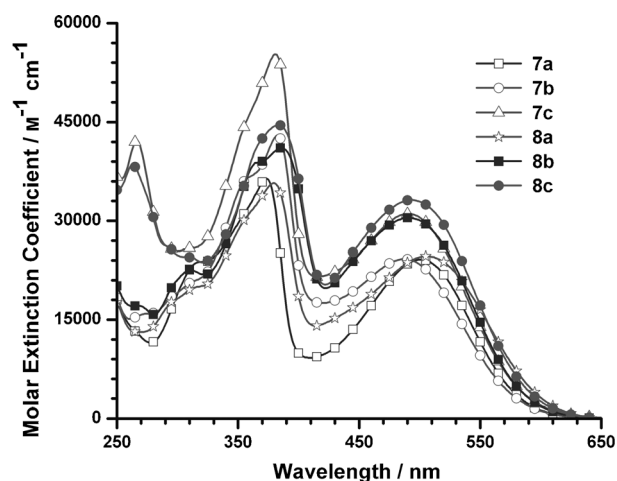


Figure 1. Absorption spectra of dyes **7** and **8** in CH_2Cl_2 .

tributed to a charge-transfer transition mixed with a delocalized π - π^* transition. In general, the features of the charge-transfer band are heavily controlled by the nature of the electron donor, the electron acceptor, and the linker. Thus, the peak positions of the lower-energy band in the dyes follow the order **8a** > **7a** > **8c** > **7c** > **8b** > **7b**. In an individual series (**7** or **8**), the charge-transfer band shifts bathochromically in the order **a** > **c** > **b**. This shift is probably due to the shorter linker length in dyes **8a** and **7a**, which is re-

sponsible for better donor-acceptor interactions when compared to other congeners that have fluorene or carbazole moieties in their conjugation pathways. The red-shift that is observed for the carbazole-linked derivatives (**8c** and **7c**) compared to their fluorene analogues (**8b** and **7b**) is attributed to the electron-rich nature of the carbazole moiety. Similarly, a slight red-shift for dyes that contain a bithiophene unit in the spacer (**8a**-**8c**) when compared to their analogous monothiophene dyes (**7a**-**7c**) is also attributed to the more electron-rich conjugation pathway, owing to the presence of an additional thiophene unit.^[20] The effect of donor-acceptor interactions on the longer-wavelength absorption can be understood by comparing the absorption wavelengths of the dyes (**7** and **8**) with that of their precursor bromides (**4**) and aldehydes (**5** and **6**; Table 1). For similar structural organization, the longer-wavelength band is red-shifted on the introduction of electron-withdrawing aldehyde or cyanoacrylic-acid units.

The molar extinction coefficient at the maximum absorption of the dyes falls in the range 24100 - $33200 \text{ M}^{-1} \text{ cm}^{-1}$, which is notably larger than those of prominent Ru-based dyes **N3**^[21] and **N719**^[22] (13900 and $14000 \text{ M}^{-1} \text{ cm}^{-1}$, respectively). The order of ϵ_{max} for the dyes that possess monothiophene and bithiophene units in the linker follows the order **7c** > **7b** > **7a** and **8c** > **8b** > **8a**, respectively. This order agrees fairly well with the general observations that the extension of conjugation and increase in electron-donating

Table 1. Optical and electrochemical properties of the dyes and their precursors.

Compound	λ_{abs} [nm] ($\epsilon \times 10^3$ [M ⁻¹ cm ⁻¹]) ^[a]	λ_{em} [nm] ^[b]	E_{ox} [mV] (ΔE_p [mV]) ^[c]	HOMO [eV] ^[d]	LUMO [eV] ^[e]	E_{0-0} [eV] ^[f]	E_{0-0}^* [V] ^[g]
4a	375 (50.1), 314 (37.6)	417	208 (90), 441 (80)	5.008	1.941	3.067	-2.09
4b	370 (40.2), 310 (27.9)	417	127 (70), 427 (74)	4.927	1.954	2.973	-2.08
4c	381 (39.9), 271 (29.6)	421	133 (76), 428 (76)	4.933	1.870	3.063	-2.16
5a	420 (26.6), 369 (33.1), 311 (24.1)	520	207 (78), 524 (80)	5.007	2.536	2.471	-1.49
5b	420 (37.1), 374 (50.1)	510	124 (68), 446 (72)	4.924	2.484	2.440	-1.55
5c	408 (35.6), 375 (49.3), 274 (36.1)	433	131 (78), 425 (72)	4.931	2.487	2.444	-1.54
6a	421 (27.1), 374 (40.6)	529	187 (74), 469 (72)	4.987	2.616	2.371	-1.41
6b	431 (42.2), 381 (50.8)	523	133 (70), 433 (70)	4.933	2.577	2.356	-1.45
6c	434 (39.7), 379 (48.3), 269 (36.1)	522	114 (80), 411 (74)	4.914	2.576	2.338	-1.45
7a	500 (24.1), 374 (36.4), 318 (23.7)	578	227.5 (91), 458.0 (84)	5.027	2.919	2.108	-1.11
7b	487 (24.2), 383 (42.9)	581	158.5 (70), 449.0 (69)	4.959	2.869	2.089	-1.16
7c	492 (31.0), 380 (45.4), 267 (42.2)	583	143.5 (75), 419 (72)	4.940	2.927	2.013	-1.09
8a	506 (24.6), 379 (35.7)	599	217.0 (78), 449.5 (89)	5.017	2.979	2.038	-1.05
8b	491 (30.4), 386 (41.1), 311 (22.5)	584	164.5 (74), 411.5 (70)	4.965	2.887	2.077	-1.14
8c	493 (33.2), 383 (44.6), 263 (38.4)	578	161 (81), 440 (82), 773	4.961	2.967	1.994	-1.05

[a] Recorded in CH₂Cl₂. [b] Recorded in toluene. [c] Potentials are quoted with reference to an internal ferrocene standard. [d] HOMO = 4.8 + E_{ox} . [e] LUMO = HOMO - E_{0-0} . [f] Obtained from the optical edge. [g] Excited-state oxidation potential with reference to NHE.

ability of the donor enhance the transition probability for the π - π^* and charge-transfer transitions, respectively.

2,7-Carbazole-bridged dyes **7c** and **8c** exhibit higher molar extinction coefficients than the other dyes in each series, owing to their electron-rich and rigid 2,7-disubstituted carbazole framework,^[23] which enhances the transition probability for both the π - π^* and charge-transfer transitions. Lower molar extinction coefficients for dyes **7a** and **8a** are attributed to non-planarity in the conjugation pathway, which retards the charge-transition probability. In between these two classes, the dyes that contain a bithiophene unit in the linker (**8**) show larger ϵ_{max} values when compared to their monothiophene analogues (**7**). This result indicates that the electron-donating ability of the π -bridge in the dyes plays an important role in increasing their light-harvesting capability.

To confirm the charge-transfer nature of the lower-energy absorption band, absorption spectra of the dyes were mea-

sured in solvents of different polarity. A representative example is illustrated in Figure 2 and the corresponding data are compiled in Table 2. All of the dyes showed negative solvatochromism for the longer-wavelength absorption band and no significant changes for the shorter-wavelength band (about 375 nm). The most red-shifted absorption was observed in CH₂Cl₂ and the absorption peak shifted to shorter wavelength on increasing the polarity. This result suggests an effective solvation of the dyes with increasing solvent polarity. The unusual red-shift in CH₂Cl₂, which caused a deviation from linearity for a plot of absorption energy against the Reichardt solvent parameter ($E_T(30)$, Figure 3), probably originates from the instant stabilization of polarizable electrons during excitation, which is induced by the larger polarizability of the solvent.^[24]

The blue-shift in polar solvents may also be contributed to by the acid-base equilibrium that is exhibited by the dyes. We speculate that the carboxylic-acid unit is partially deprotonated in polar solvents that are capable of abstracting the acidic hydrogen atom, either by hydrogen bonding or owing to

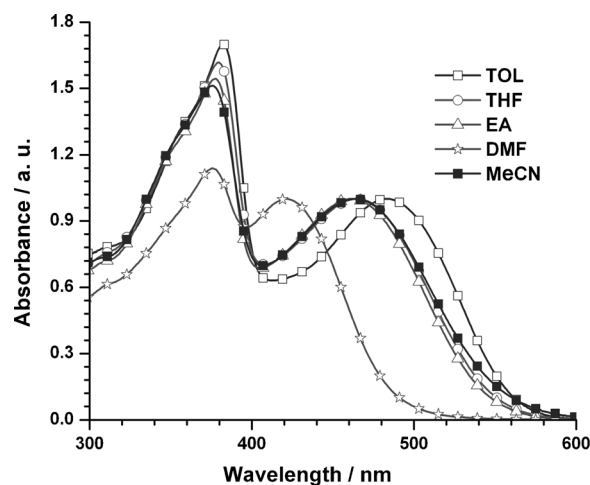
Figure 2. Absorption spectra of dye **7c** in various solvents.

Table 2. Absorption data for the dyes in various solvents.^[a]

Dye	λ_{abs} [nm] ($\epsilon \times 10^3$ [$\text{M}^{-1} \text{cm}^{-1}$]) ^[b]								
	TOL	TOL+TFA	TOL+TEA	CH ₂ Cl ₂ +TFA	CH ₂ Cl ₂ +TEA	THF	EtOAc	DMF	MeCN ^[c]
7a	489 (29.6),	530 (28.2),	434 (32.3),	513 (23.7),	438 (28.7),	470 (32.9),	470 (28.2),	421 (32.1),	477,
	375 (41.2),	376 (29.9),	374 (39.9),	373 (37.7),	372 (38.3),	372 (48.1),	370 (38.4),	370 (37.9),	368,
	315 (26.2)	314 (24.2)	316 (27.6)	316 (24.4)	315 (27.4)	316 (30.7)	313 (24.7)	312 (26.6)	315
7b	477 (28.0),	512 (19.2),	428 (32.7),	499 (24.8),	433 (43.8),	458 (32.0),	456 (30.7),	420 (46.7),	427,
	383 (38.5)	384 (36.5)	380 (41.3)	383 (41.5)	379 (59.3)	380 (50.6)	378 (46.5)	377 (55.6),	378
								312 (29.8)	
7c	483 (28.5),	520 (24.1),	431 (38.1),	504 (33.1),	435 (40.5),	465 (37.8),	461 (34.3),	422 (53.1),	463,
	382 (48.6)	385 (41.6)	319 (47.9)	381 (56.3),	377 (54.4),	380 (61.1)	378 (52.9)	376 (60.4),	376
				267 (45.1)	265 (39.8)			310 (32.4)	
8a	497 (25.7),	528 (28.2),	447 (33.9),	515 (26.2),	449 (33.5),	478 (29.6),	477 (34.9),	441 (40.1),	482,
	381 (34.4),	381 (28.1),	379 (38.6),	379 (34.5)	378 (41.3)	378 (40.0)	376 (45.5)	376 (60.4),	375
	315 (18.9)	308 (17.7)	318 (22.1)					315 (26.1)	
8b	484 (34.3),	499 (30.9),	441 (43.9),	492 (34.4),	444 (49.3),	468 (44.2),	465 (44.1),	437 (51.3),	456,
	387 (43.8)	387 (42.0)	384 (43.8)	386 (41.9),	383 (52.9)	384 (54.5),	382 (52.6),	384 (49.9),	382,
				310 (24.3)		309 (28.1)	308 (26.9)	310 (26.1)	311
7a	489 (29.6),	530 (28.2),	434 (32.3),	513 (23.7),	438 (28.7),	470 (32.9),	470 (28.2),	421 (32.1),	477,
	375 (41.2),	376 (29.9),	374 (39.9),	373 (37.7),	372 (38.3),	372 (48.1),	370 (38.4),	370 (37.9),	368,
	315 (26.2)	314 (24.2)	316 (27.6)	316 (24.4)	315 (27.4)	316 (30.7)	313 (24.7)	312 (26.6)	315
7b	477 (28.0),	512 (19.2),	428 (32.7),	499 (24.8),	433 (43.8),	458 (32.0),	456 (30.7),	420 (46.7),	427,
	383 (38.5)	384 (36.5)	380 (41.3)	383 (41.5)	379 (59.3)	380 (50.6)	378 (46.5)	377 (55.6),	378
								312 (29.8)	
8c	455 (30.5),	475 (27.5),	442 (42.4),	502(32.2),	448 (45.1),	459 (32.6),	446 (29.5),	437 (54.3),	436,
	383 (44.3)	384 (45.0)	381 (49.3)	380 (41.3)	381 (49.7)	382 (43.7)	379 (39.4)	379 (54.2)	376

[a] Abbreviations: toluene (TOL), trifluoroacetic acid (TFA), triethylamine (TEA). [b] Recorded at the concentration of 2.0×10^{-5} M. [c] Molar extinction coefficient values could not be obtained owing to poor solubility.

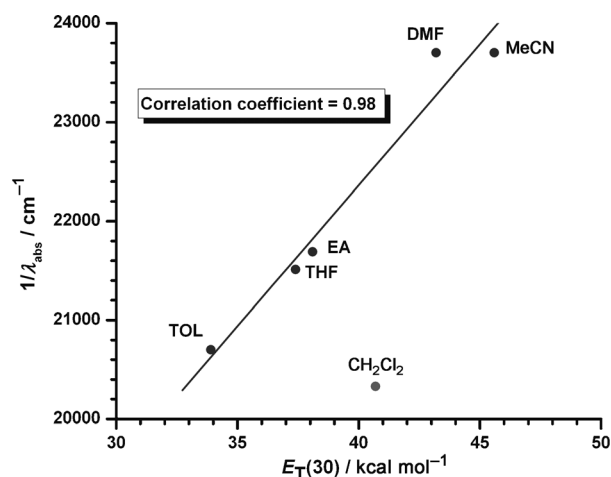


Figure 3. Correlation between the absorption maxima for dye **7c** in different solvents with the $E_T(30)$ parameter.

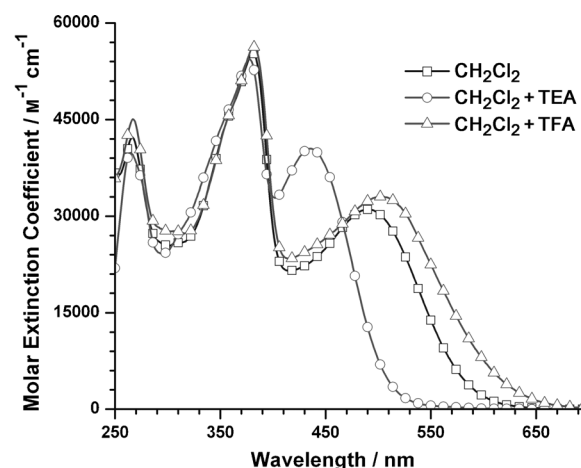


Figure 4. Absorption spectra of dye **7c** in CH₂Cl₂ in the presence of TEA or TFA.

the basic nature of the solvent. This abstraction may, in turn, impede the donor–acceptor interactions in the dye and produce a hypsochromic shift of the charge-transfer transition.^[25] This theory is supported by the addition of triethylamine (TEA) or trifluoroacetic acid (TFA) to solutions of the dyes in toluene/CH₂Cl₂. The addition of TEA leads to a significant blue-shift in the absorption, owing to the ineffective charge transfer that is caused by deprotonation of the carboxylic acid, whilst TFA causes a red-shift (Figure 4). The absorption spectra of the dyes in *N,N*-dimethylformamide (DMF) displayed a prominent blue-shift for the

charge-transfer transition compared to those in other solvents, which was consistent with the basicity of DMF.

It is interesting to compare the optical properties of dyes **7a** and **8a** with those of (*E*)-2-cyano-3-(4-((7-(diphenylamino)-9,9-diethyl-9*H*-fluoren-2-yl)(phenyl) amino) phenyl)acrylic acid (**JD1**),^[13] which we reported previously. The insertion of a thiophene (**7a**) or bithiophene moiety (**8a**) into the conjugation pathway between the donor and acceptor triggers a red-shift of 53 and 59 nm, respectively. The effect of the auxiliary donor group is evident by comparing dye **7a** with (*E*)-2-cyano-3-(5-(4-(diphenylamino)phenyl)thiophen-

2-yl)acrylic acid^[26] and dye **8a** with (*E*)-2-cyano-3-(5'-(4-(diphenylamino)phenyl)-[2,2'-bithiophen]-5-yl)acrylic acid.^[27] The presence of an additional diphenylaminofluorene donor group leads to hyperchromism and a red-shift of the charge-transfer transition. Similar effects have also been observed for the fluorene-conjugated derivatives (**7b** and **8b**) when compared with their analogous monoamine derivatives. All of these observations clearly indicate that the extension of conjugation between the donor and the acceptor, and the introduction of an additional donor in the form of diphenylaminofluorene, are beneficial for the light-harvesting properties.

The dyes are weakly emissive in toluene (Table 1) and the emission wavelength is insensitive to the nature of the bridging segment. The emission of the dyes is completely quenched when dissolved in polar solvents, such as MeCN, CH₂Cl₂, etc. This result probably indicates the presence of a noticeable dipole in the dye molecules, owing to extensive polarization, which may interact with the solvent dipole and facilitate nonradiative relaxation of the excited state by an electron-transfer mechanism.^[28]

Electrochemical Properties

Cyclic voltammetry was carried out to determine the oxidation potentials of the dyes in the ground (E_{ox}) and excited states (E_{ox}^*). The excited-state oxidation potential, E_{ox}^* , can be obtained by subtracting the 0–0 transition energy (E_{0-0}) from E_{ox} and the required E_{0-0} value is derived from the absorption edge. Two quasi-reversible one-electron oxidations were detected for the dyes (Figure 5). These oxidation potentials are more positive than the ferrocene/ferrocenium redox couple.^[29] The first oxidation (131.0–227.5 mV) is attributed to the removal of an electron from the auxiliary donor. The second oxidation wave, at higher potential, is attributed to the oxidation of the amine donor, which is in direct electronic communication with the cyanoacrylic-acid acceptor unit. Both oxidations follow a similar trend, owing to the variation in the nature of the conjugation segment. The oxidation potentials follow the order $c < b < a$ for both

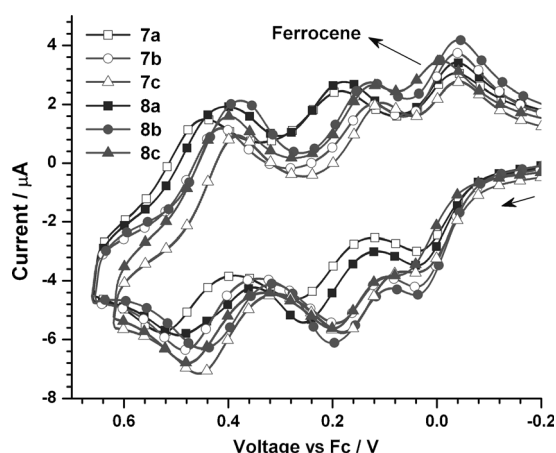


Figure 5. Cyclic voltammograms of dyes **7** and **8** in CH₂Cl₂.

series (**7** and **8**). Apparently, the electronic communication between the amine donor and the cyanoacrylic-acid acceptor significantly affects the oxidation potential: The stronger interactions result in less-facile oxidation of the aryl amine. Stronger donor–acceptor interactions were speculated for dyes **7a** and **8a** based on their absorption spectra (see below). Longer conjugating segments, such as fluorene and carbazole moieties, lessened the interactions between the amine and the cyanoacrylic acid and cathodically shifted the oxidation potentials of the corresponding dyes, **7b**, **8b**, **7c**, and **8c**, when compared to the dyes with phenylene linkages (**7a** and **8a**). The more electron-rich fluorene and carbazole groups, compared to the phenyl unit, may be also responsible for this shift. Consequently, carbazole, which is sufficiently electron rich, facilitates the oxidation of dyes **7c** and **8c** by increasing the electron density over the donor amine moieties. The oxidation potentials are in the range 0.91–1.00 V versus the normal hydrogen electrode (NHE) and the E_{ox}^* values for the dyes are between –1.05 and –1.19 V versus NHE. These values are favorable for facile electron injection from the dye into the conduction band of TiO₂ and for regeneration of the oxidized dyes by the I₂/I[–] electrolyte.^[30] The oxidation potentials are significantly lower than that of the closely related dyes that contain monoamine donors and clearly reveal the role of the auxiliary donor.^[13,26,27]

The effect of the addition of TFA on the electrochemical properties of the dyes was also analyzed by CV (Figure 6). A strong acid, such as TFA, is expected to either shift the acid–base equilibrium of the dyes toward their acidic form or to protonate the amine unit. Both effects, in principle, could make the amines difficult to oxidize. As expected, the redox potentials that correspond to both oxidations of the dyes increased upon the addition of TFA to the dye solutions (Figure 6). This result confirms that the charge-transfer interactions are spread over the entire molecule. However, the positive shift for the first oxidation potential is less pronounced than that of the second oxidation potential. This result suggests that the donor amine moiety, which is adja-

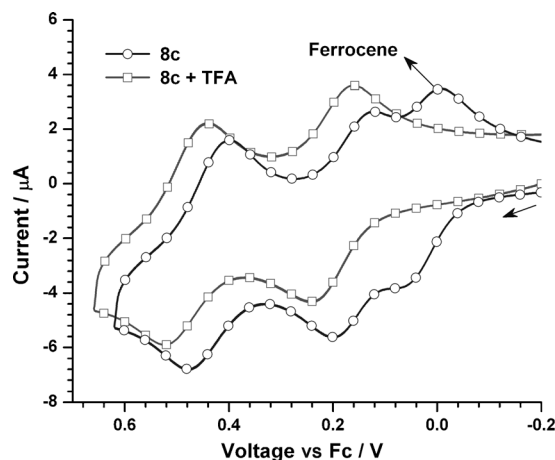


Figure 6. Cyclic voltammograms of dye **8c** in CH₂Cl₂ before and after the addition of TFA.

Table 3. Computed vertical transition energies, oscillator strengths (f), and their assignment for the dyes.^[a]

Dye	B3LYP (vacuum)			Theory			MP2K (THF)		
	λ_{\max} [nm]	f	Configuration	λ_{\max} [nm]	f	Configuration	λ_{\max} [nm]	f	Configuration
7a	587	0.36	HOMO→LUMO (100%)	426	1.03	HOMO→LUMO (71%), HOMO-1→LUMO (22%)	452	1.18	HOMO→LUMO (67%), HOMO-1→LUMO (26%)
7b	639	0.30	HOMO→LUMO (99%)	433	1.02	HOMO→LUMO (73%), HOMO-1→LUMO (16%)	454	1.12	HOMO→LUMO (70%), HOMO-1→LUMO (17%)
7c	634	0.27	HOMO→LUMO (99%)	428	0.96	HOMO→LUMO (74%), HOMO-1→LUMO (16%)	449	1.13	HOMO→LUMO (71%), HOMO-1→LUMO (16%)
8a	645	0.38	HOMO→LUMO (99%)	450	1.26	HOMO→LUMO (64%), HOMO-1→LUMO (25%)	477	1.43	HOMO→LUMO (64%), HOMO-1→LUMO (25%)
8b	680	0.28	HOMO→LUMO (99%)	447	1.35	HOMO→LUMO (61%), HOMO-1→LUMO (19%), HOMO-2→LUMO (13%)	469	1.57	HOMO→LUMO (54%), HOMO-1→LUMO (21%), HOMO-2→LUMO (18%)
8c	681	0.24	HOMO→LUMO (99%)	445	1.26	HOMO→LUMO (63%), HOMO-1→LUMO (19%), HOMO-2→LUMO (12%)	467	1.52	HOMO→LUMO (56%), HOMO-1→LUMO (21%), HOMO-2→LUMO (13%)

[a] Contributions of less than 10% are omitted.

cent to the cyanoacrylic acid unit, is largely affected by the addition of TFA. Because it is less basic than the secondary donor amine, it is safe to conclude that the addition of TFA leads to the population of the more neutral acidic form of the dyes in solution.

Electronic Structure of the Dyes

The electronic structures of the dyes were simulated in a vacuum by using density functional theory (DFT)^[31] with the B3LYP^[32] model and the 6-31G** basis set, as implemented in Gaussian 09.^[33] The lowest-energy transitions that were derived from the theoretical computations, along with their oscillator strengths and their compositions in terms of molecular orbitals, are listed in Table 3. The electronic distributions in the HOMO and LUMO for the selected dyes are shown in Figure 7. The HOMO is mainly spread on the 2,7-diarylamino-fluorene unit with a slight delocalization over the phenyl, fluorene, and carbazole moieties. The LUMO is mainly constructed from the cyanoacrylic-acid segment and is contributed to, to some extent, by the thiophene moiety. There is clear charge separation between the

HOMO and the LUMO, which suggests better donor-acceptor interactions in the molecules. The higher-wavelength electronic transitions for the dyes, as predicted theoretically, have major contributions from the HOMO-to-LUMO electronic excitation and possess reasonable oscillator strength. In view of this result, the longer-wavelength absorption for the dyes may be safely assigned to a charge-transfer transition. From the electronic distributions of the molecular orbitals that are involved in the shorter-wavelength absorptions (not shown); these absorptions can be inferred to as originating from localized π - π^* transitions. The peak positions as predicted by the MPW1K^[34] model closely resembled those observed in THF (Table 3). The experimental trend for the HOMO (**a** > **b** > **c**) of the dyes is consistent with the theoretical values and, in turn, supports a progressive change in the electron richness of the bridging segment.

Characteristics of the DSSCs

The photovoltaic performance of the newly synthesized dyes (**7** and **8**) were evaluated by using the Grätzel photoelectrochemical cell.^[30] The photovoltaic performance parameters for the dyes are collected in Table 4. Figure 8 shows the I - V characteristics and incident photon-to-current conversion efficiency (IPCE) action spectra for the DSSCs that were based on these dyes. The IPCE spectra show maximum conversion efficiencies in the region 400–550 nm. The IPCEs of dyes **7b** and **8b** are more than 80% and 70%, respectively, in the range 400–450 nm. The IPCEs for dyes **7a**, **8a**, **7c**, and **8c** reach 67, 67, 66, and 66.5% at 440 nm, respectively. The onset IPCE for dyes **7a–8a** and **7b–8c** starts close to about 680 nm.

The short-circuit photocurrent density and efficiency for the devices increase in the order **7c** < **7a** < **7b** and **8c** < **8a** < **8b**. The short-circuit current is related to the molar extinction coefficient of the dyes. For dyes **7b** and **8b**, a higher molar extinction coefficient yields a higher short-circuit current. However, for dyes **7c** and **8c**, the short-circuit current

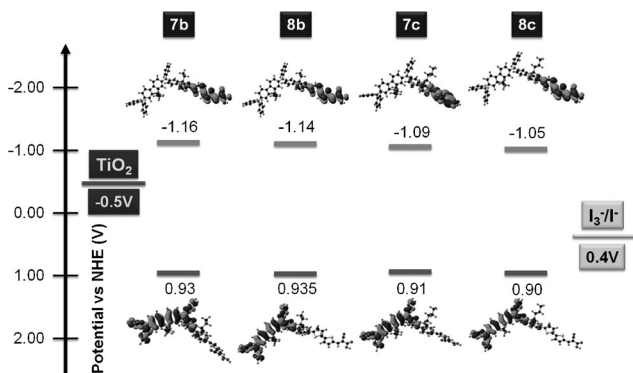
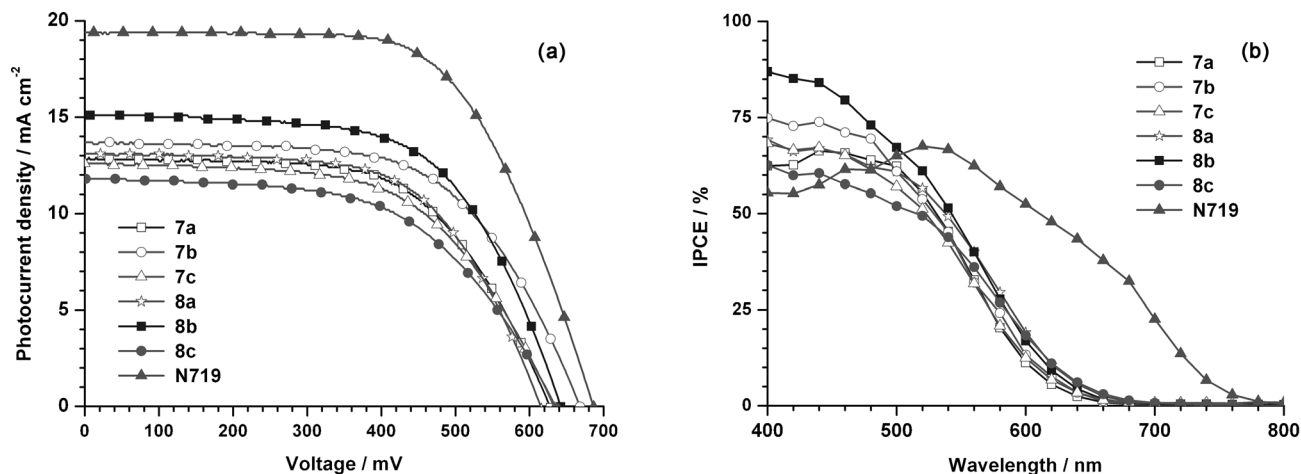


Figure 7. Energy-level diagram of the frontier molecular orbitals of dyes **7b**, **7c**, **8b**, and **8c**.

Table 4. Photovoltaic-performance parameters of the dyes.

Dye	V_{oc} [mV]	J_{sc} [mA cm^{-2}]	ff	η [%]	R_{rec} [Ω]	R_{ct2} [Ω]	τ_e [ms]
7a	628	12.8	0.60	4.85	20.75	19.43	4.63
7b	668	13.7	0.61	5.52	32.50	18.49	33.76
7c	634	12.6	0.58	4.62	22.61	19.28	8.41
8a	616	13.1	0.61	4.94	15.50	18.68	5.65
8b	642	15.1	0.61	5.91	16.50	17.92	8.41
8c	636	11.8	0.56	4.20	25.22	20.27	5.65
N719	687	19.4	0.63	8.36	31.24	9.05	15.27

Figure 8. a) I - V characteristics and b) IPCE plots for the devices under illumination at 100 mW cm^{-2} .

is low, irrespective of their high molar extinction coefficient. This result may be ascribed to an ineffective overlap of the LUMO level of the dye with the conduction band of TiO_2 , which probably retards electron injection.^[35] Dyes **7a** and **8a** show lower efficiencies than dyes **7b** and **8b**, owing to the lower molar coefficients of the former dyes; in addition, they show broader absorption bands than the latter dyes when adsorbed onto a TiO_2 surface. Thus, the aggregation-induced quenching in the excited state may lead to a weaker light-harvesting ability of the dyes.^[36]

Electrochemical Impedance Spectroscopy

Because the electronic coupling between the sensitizer and the TiO_2 nanoparticles can alter the quasi-Fermi level of TiO_2 , the V_{oc} value can be different for cells that are made from different sensitizers. To elucidate the effect of the nature of the π -linker on the V_{oc} value, electrochemical impedance spectroscopy (EIS) measurements were conducted. Figure 9 shows Nyquist plots for DSSCs that were constructed from the sensitizers under dark conditions. In general, the Nyquist plots show three semicircles, which are assigned to the electrochemical reaction at the Pt/electrolyte interface, charge transfer at the TiO_2 /dye/electrolyte interface, and to the Warburg diffusion process (I^-/I_3^-) in the electrolyte.^[37] In our DSSCs, we only observed two semicircles. We assume that, in these DSSCs, the conventional diffusion resistance of the redox couple is greatly overlapped by the

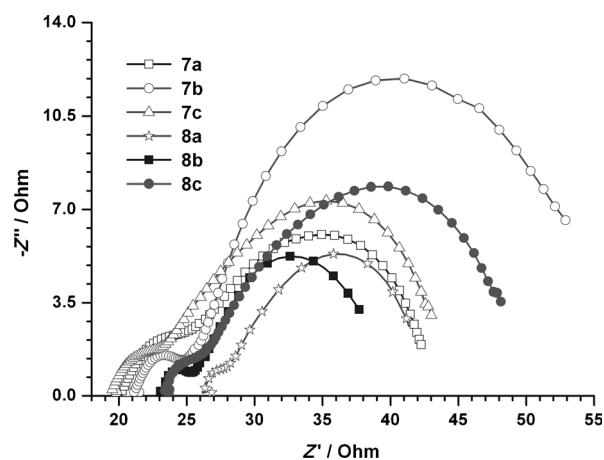


Figure 9. Nyquist plots for the DSSCs that were fabricated by using the dyes under dark conditions.

charge-transfer resistance because of the short length of available I^- diffusion with the thin spacer and owing to the low viscosity of the solvents that are used in the electrolyte. The smaller semicircle corresponds to charge-transfer resistance at the counter electrode and the larger semicircle corresponds to charge-transfer resistance at the TiO_2 /dye/electrolyte interface (R_{rec}). The radius of this semicircle follows the order $8a < 8b < 7a < 7c < 8c < 7b$, which indicates that dye **7b** possesses the highest charge-recombination resist-

ance, whereas dye **8a** has the lowest resistance. This order is largely in agreement with the trend for V_{oc} (**8a** < **7a** < **7c** < **8c** < **8b** < **7b**), with the exception of dye **8b**. Smaller R_{rec} values indicate faster charge recombination and larger dark current, which result in a comparatively small open-circuit voltage for dye **8a**. The open-circuit voltage in DSSCs is mainly determined by the conduction-band edge of TiO_2 , because the redox potential of the electrolyte is unlikely to undergo changes between devices that are fabricated under similar conditions. Factors that can influence the electron density on the TiO_2 surface can significantly affect the V_{oc} value. The oxidation potential of the dye and the charge-recombination resistance can alter the electron density in TiO_2 . Dyes that undergo oxidation more easily may increase the polarizability of the molecule and enhance the electron density on TiO_2 . The lowest oxidation potentials, for dyes **7c**, **7b**, and **8c**, support this argument. The reason for the higher V_{oc} value for dye **8b**, despite it having lower charge-recombination resistance in the device, is unclear.

Upon illumination at 100 mW cm^{-2} under open-circuit conditions, from the radius of the intermediate-frequency semicircle in the Nyquist plot (Figure 10a), we found that the electron-transport resistance (R_{ct2}) followed the order

8c > **7a** > **7c** > **8a** > **7b** > **8b** > **N719**. We expect that a lower value of electron-transfer resistance would support the electron collection and, consequently, would play an important role in increasing the efficiency of a cell. The electron lifetime can be extracted from the angular frequency (ω_{min}) at the mid-frequency peak in the Bode phase plot (Figure 10b) by using $\tau_e = 1/\omega_{min}$.^[38] The obtained τ_e values follow the order **7b** > **8b** > **7c** > **8c** \approx **7a** > **8a**, which is consistent with the order of the V_{oc} values (see above). The increase in the electron lifetimes for the devices that are based on fluorene-containing dyes (**7b** and **8b**) suggests a more effective suppression of the back reaction of injected electrons with I_3^- ions in the electrolyte, which leads to an improvement in both the J_{sc} and V_{oc} values, as well as to a substantial enhancement in the PCE of the DSSC. This result may suggest that the presence of the fluorene moiety in the spacer is beneficial for electronic coupling and for the suppression of back-electron transfer when compared to the phenyl/carbazole moieties.

Conclusions

We have developed several new organic dyes that contain a fluorene-2,7-diamine-based donor and a cyanoacrylic-acid acceptor; these units were bridged by various aromatic conjugated segments that were composed of benzene, fluorene, carbazole, and thiophene units. These dyes were characterized by optical spectroscopy, cyclic voltammetry, and TDDFT computations. The absorption and electrochemical properties of the dyes were in accordance with the electron-donating ability of the conjugating segment. Consequently, the 2,7-carbazole-bridged dyes exhibited red-shifted absorptions and lower oxidation potentials than their corresponding fluorene- and phenylene-bridged dyes. The enhanced power-conversion efficiencies that were observed for the fluorene-bridged dyes were attributed to their broader and more intense absorption profiles. Their enhanced optical properties contributed to the increase in their photocurrent density and their comparatively larger HOMO value facilitated the regeneration of the dyes by the electrolyte, as well as suppressing the back reaction of the injected electrons with the electrolyte constituents. Despite the longer-wavelength absorption and reasonable optical density that was observed for the carbazole-bridged dyes, their relatively lower power-conversion efficiencies were ascribed to the poor alignment of the LUMO level of the dye, which probably inhibited the electron injection into the TiO_2 conduction band. The success of this design strategy to improve device performance indicates that more detailed studies on the structure–property relationships in the organic dyes is essential to understand the more complicated physicochemical processes that are involved in DSSCs and to optimize them to increase their power-conversion efficiency.

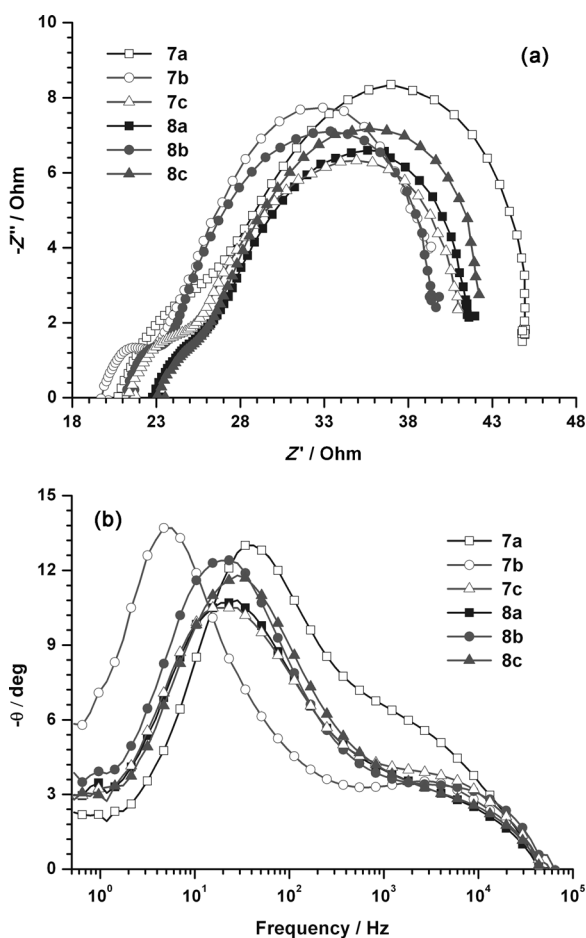


Figure 10. a) Nyquist and b) Bode phase plots for the devices that were fabricated by using dyes under illumination at 100 mW cm^{-2} .

Experimental Section

General Methods

All reactions and manipulations were carried out under a N₂ atmosphere by using standard Schlenk techniques. Solvents were dried according to standard procedures. Column chromatography was performed on either 100–200 mesh silica gel or on neutral alumina as the stationary phase (column length: 30 cm, diameter: 2.0 cm). ¹H and ¹³C NMR spectroscopy were measured on a 500 MHz spectrometer (Bruker). MS was recorded in positive-ion mode on an ESI TOF high-resolution mass spectrometer (Bruker Daltonics). Cyclic voltammetry (CH Instruments) was carried out at RT on a conventional three-electrode configuration that consisted of a glassy carbon working electrode, a platinum-wire auxiliary electrode, and a non-aqueous Ag/AgNO₃ reference electrode. *E*_{1/2} values were determined as 1/2(*E*_{p^a}+*E*_{p^c}), where *E*_{p^a} and *E*_{p^c} are the anodic and cathodic peak potentials, respectively; the potentials are quoted against an internal ferrocene standard. CH₂Cl₂ was used as the solvent in all of the experiments and the supporting electrolyte was 0.1 M tetrabutylammonium perchlorate. Electronic absorption spectra were obtained on a UV/Vis spectrophotometer (Shimadzu) by using freshly prepared solutions.

Synthesis of 9,9-diethyl-N²,N⁷,N⁷-triphenyl-9H-fluorene-2,7-diamine (2)

In a pressure tube, 7-bromo-9,9-diethyl-*N,N*-diphenyl-9H-fluorene-2-amine (3.3 g, 7.0 mmol) and aniline (0.72 g, 7.7 mmol) were mixed with sodium *tert*-butoxide (1.2 g, 12.4 mmol), [Pd(dba)₂] (dba = (1*E*,4*E*)-1,5-diphenylpenta-1,4-dien-3-one; 100 mg, 0.18 mmol), and 1,2-bis(diphenylphosphino)ferrocene (dppf; 100 mg, 0.18 mmol) in toluene (10 mL) under a nitrogen atmosphere. The mixture was heated at 80°C for 36 h. After the completion of the reaction, the volatile compounds were removed by evaporation. The residue was triturated with water and extracted with CH₂Cl₂. The combined organic layer was dried over anhydrous sodium sulfate and evaporated under vacuum to produce a crude product, which was adsorbed onto neutral alumina and purified by column chromatography (hexanes/CH₂Cl₂). White solid; yield: 1.72 g (51%); m.p. 122–124°C; ¹H NMR (500 MHz, CDCl₃): δ = 7.52 (d, *J* = 8.0, 1H), 7.24–7.31 (m, 7H), 6.93–7.17 (m, 13H), 5.30 (s, 1H), 1.85–1.92 (m, 4H), 0.39–0.45 ppm (m, 6H); ¹³C NMR (125 MHz, CDCl₃): δ = 151.4, 151.2, 147.2, 146.1, 145.9, 136.8, 132.07, 132.05, 129.3, 129.1, 124.7, 124.7, 123.9, 123.7, 122.9, 122.9, 122.4, 120.0, 119.9, 119.6, 119.4, 114.4, 114.3, 56.0, 32.5, 8.6 ppm; HRMS (ESI): *m/z* calcd for C₃₅H₃₂N₂: 480.2565 [M+H]⁺; found: 480.2560.

Synthesis of N²-(4-bromophenyl)-9,9-diethyl-N²,N⁷,N⁷-triphenyl-9H-fluorene-2,7-diamine (4a)

In a round-bottomed flask, 9,9-diethyl-N²,N²,N⁷,N⁷-tetraphenyl-9H-fluorene-2,7-diamine (1.0 g, 1.79 mmol) and *N*-bromosuccinimide (0.36 g, 1.87 mmol) were dissolved in CCl₄ (15 mL). This mixture was heated at reflux for 4 h, cooled to RT, and filtered. The solvent was evaporated from the filtrate and the solid was recrystallized from EtOH. White solid; yield: 0.75 g (65%); m.p. 118–120°C; ¹H NMR (500 MHz, CDCl₃): δ = 7.40–7.42 (m, 2H), 7.20–7.26 (m, 3H), 7.16–7.18 (m, 5H), 6.87–7.03 (m, 15H), 1.71–1.74 (m, 4H), 0.26–0.30 ppm (m, 6H); ¹³C NMR (125 MHz, CDCl₃): δ = 151.4, 151.2, 147.5, 147.2, 146.7, 146.1, 145.9, 137.1, 136.8, 132.2, 132.07, 132.05, 129.3, 129.1, 124.7, 124.7, 123.9, 123.7, 122.94, 122.87, 122.4, 120.0, 119.9, 119.7, 119.6, 119.4, 114.4, 114.3, 56.1, 56.0, 32.5, 8.6 ppm; HRMS (ESI): *m/z* calcd for C₄₁H₃₃BrN₂: 635.2056 [M+H]⁺; found: 635.2056.

General Synthesis of the Bromo Derivatives of the Diamines (4b and 4c)

An appropriate aryldibromide (2,7-dibromo-9,9-diethyl-9H-fluorene or 2,7-dibromo-9-butyl-9H-carbazole; 5.0 mmol) was mixed with sodium *tert*-butoxide (0.72 g, 7.5 mmol), [Pd(dba)₂] (dba = (1*E*,4*E*)-1,5-diphenylpenta-1,4-dien-3-one; 29 mg, 0.05 mmol), 1,2-bis(diphenylphosphino)ferrocene (dppf; 28 mg, 0.05 mmol), and 9,9-diethyl-N²,N²,N⁷-triphenyl-9H-fluorene-2,7-diamine (1.20 g, 2.5 mmol) in toluene (10 mL) under a nitrogen atmosphere. This mixture was heated at 80°C for 36 h. After the completion of the reaction, the volatile compounds were removed by evaporation. The residue was triturated with water and extracted with

CH₂Cl₂. The combined organic layer was dried over anhydrous sodium sulfate and evaporated under vacuum to afford the crude product, which was adsorbed onto neutral alumina and purified by column chromatography (hexanes/CH₂Cl₂). The desired bromo derivative was collected as the second fraction after recovery of the unreacted excess aryldibromide.

N²-(7-Bromo-9,9-diethyl-9H-fluorene-2-yl)-9,9-diethyl-N²,N⁷,N⁷-triphenyl-9H-fluorene-2,7-diamine (4b)

Compound **4b** was synthesized from 2,7-dibromo-9,9-diethyl-9H-fluorene and 9,9-diethyl-N²,N²,N⁷-triphenyl-9H-fluorene-2,7-diamine according to the general procedure described above. White solid; yield: 1.11 g (57%); m.p. 124–126°C; ¹H NMR (500 MHz, CDCl₃): δ = 7.39–7.53 (m, 6H), 7.22–7.23 (m, 6H), 6.97–7.15 (m, 15H), 1.77–1.92 (m, 8H), 0.33–0.39 ppm (m, 12H); ¹³C NMR (125.77 MHz, CDCl₃): δ = 151.7, 139.4, 130.2, 126.2, 121.5, 121.1, 56.7, 32.6, 8.4 ppm; HRMS (ESI): *m/z* calcd for C₅₂H₄₇BrN₂: 779.2995 [M+H]⁺; found: 779.2996.

N²-(7-Bromo-9-butyl-9H-carbazol-2-yl)-9,9-diethyl-N²,N⁷,N⁷-triphenyl-9H-fluorene-2,7-diamine (4c)

Compound **4c** was synthesized from 2,7-dibromo-9-butyl-9H-carbazole and 9,9-diethyl-N²,N²,N⁷-triphenyl-9H-fluorene-2,7-diamine according to the general procedure described above. White solid; yield: 1.28 g (66%); m.p. 140–142°C; ¹H NMR (500 MHz, CDCl₃): δ = 7.87 (d, *J* = 8.5 Hz, 1H), 7.82 (d, *J* = 8.5 Hz, 1H), 7.49–7.52 (m, 2H), 7.46 (d, *J* = 1.0 Hz, 1H), 7.26–7.30 (m, 4H), 7.23–7.25 (m, 3H), 7.17 (d, *J* = 8.5 Hz, 2H), 7.07–7.14 (m, 8H), 6.98 (m, 5H), 4.06 (t, *J* = 7.0 Hz, 2H), 1.81 (dd, *J* = 14.5 Hz, 7.5 Hz, 4H), 1.71 (t, *J* = 7.5 Hz, 2H), 1.29 (dd, *J* = 15.5 Hz, 7.5 Hz, 2H), 0.85–0.88 (m, 3H), 0.39 ppm (t, *J* = 7.5 Hz, 6H); ¹³C NMR (125 MHz, CDCl₃): δ = 151.32, 151.25, 148.5, 148.1, 147.0, 146.8, 146.6, 141.8, 141.7, 136.7, 136.7, 129.2, 123.9, 122.4, 122.1, 122.0, 120.83, 120.76, 119.80, 119.6, 119.5, 118.3, 117.7, 116.9, 111.6, 104.2, 56.1, 42.8, 32.6, 31.0, 20.5, 13.8, 8.6 ppm; HRMS (ESI): *m/z* calcd for C₅₁H₄₆BrN₃: 780.2948 [M+H]⁺; found: 780.2945.

5-(4-((7-(Diphenylamino)-9,9-diethyl-9H-fluorene-2-yl)(phenyl)amino)phenyl)-thiophene-2-carbaldehyde (5a)

A solution of (5-(1,3-dioxolan-2-yl)thiophen-2-yl)tributylstannane (0.65 mmol) and N²-(4-bromophenyl)-9,9-diethyl-N²,N⁷,N⁷-triphenyl-9H-fluorene-2,7-diamine (**4a**; 0.35 g, 0.55 mmol) in dry DMF (4 mL) was degassed with nitrogen, followed by the addition of bis(triphenylphosphine)dichloropalladium(II) ([Pd(PPh₃)₂Cl₂]; 4 mg, 1 mol%). The reaction mixture was heated at 80°C for 24 h under a nitrogen atmosphere. After that, the mixture was poured into water and extracted with CH₂Cl₂. The organic layer was washed with brine and water and dried over anhydrous Na₂SO₄. The solvent was evaporated and the solid residue was dissolved in glacial acetic acid (5 mL). The solution was stirred for 30 min at 60°C, then water (10 mL) was added. Heating was continued for a further 6 h. After cooling to RT, water was added and the mixture was extracted with CH₂Cl₂. The organic layer was washed with a liberal amount of water and dried over anhydrous Na₂SO₄. After removal of the solvent under vacuum, the residue was purified by column chromatography on silica gel (hexanes/CH₂Cl₂). Orange solid; yield: 0.165 g (45%); m.p. 117–120°C; ¹H NMR (500 MHz, CDCl₃): δ = 9.86 (s, 1H), 7.71 (d, *J* = 3.5 Hz, 1H), 7.50–7.54 (m, 4H), 7.27–7.34 (m, 4H), 7.23–7.25 (m, 2H), 6.97–7.17 (m, 16H), 1.83 (dd, *J* = 14.0 Hz, 7.0 Hz, 4H), 0.39 ppm (t, *J* = 7.0 Hz, 6H); ¹³C NMR (125 MHz, CDCl₃): δ = 182.6, 154.7, 151.6, 151.4, 149.4, 148.1, 147.2, 146.9, 145.5, 141.3, 137.8, 136.4, 132.2, 129.5, 129.2, 127.3, 125.9, 124.9, 124.8, 124.7, 124.7, 124.1, 123.82, 123.75, 123.7, 123.6, 122.8, 122.5, 122.2, 122.1, 120.4, 120.1, 119.4, 56.2, 56.1, 32.6, 8.6 ppm; IR (KBr): $\tilde{\nu}$ = 1658 cm⁻¹ (C=O); HRMS (ESI): *m/z* calcd for C₄₆H₃₈N₂O₂: 667.2778 [M+H]⁺; found: 667.2782.

5-(7-((7-(Diphenylamino)-9,9-diethyl-9H-fluorene-2-yl)(phenyl)amino)-9,9-diethyl-9H-fluorene-2-yl)thiophene-2-carbaldehyde (5b)

Compound **5b** was synthesized according to a procedure that was similar to that of compound **5a**, except that compound **4b** was used in the place of compound **4a**. Orange solid; yield: 0.28 g (62%); m.p. 138–141°C; ¹H NMR (500 MHz, CDCl₃): δ = 9.89 (s, 1H), 7.75 (d, *J* = 4.0 Hz, 1H),

7.63–7.67 (m, 2H), 7.56–7.59 (m, 2H), 7.49–7.52 (m, 2H), 7.45 (d, $J=4.0$ Hz, 1H), 7.26–7.30 (m, 2H), 7.23–7.26 (m, 4H), 7.16 (d, $J=7.5$ Hz, 2H), 6.98–7.12 (m, 13H), 1.96–2.03 (m, 2H), 1.77–1.92 (m, 6H), 0.36–0.40 ppm (m, 12H); ^{13}C NMR (125 MHz, CDCl_3): $\delta=182.6, 151.6, 151.2, 151.0, 150.6, 148.1, 147.9, 146.44, 146.36, 143.0, 141.6, 137.4, 136.6, 136.5, 130.6, 129.1, 129.0, 125.5, 123.9, 123.7, 123.5, 123.4, 122.6, 122.5, 122.2, 120.6, 120.4, 119.7, 119.4, 119.1, 118.0, 56.1, 56.0, 32.6, 32.5, 8.5$ ppm; IR (KBr): $\tilde{\nu}=1636\text{ cm}^{-1}$ (C=O); HRMS (ESI): m/z calcd for $\text{C}_{57}\text{H}_{50}\text{N}_2\text{OS}$: 811.3717 $[\text{M}+\text{H}]^+$; found: 811.3716.

5-(9-Butyl-7-((7-(diphenylamino)-9,9-diethyl-9H-fluoren-2-yl)(phenyl)amino)-9H-carbazol-2-yl)thiophene-2-carbaldehyde (**5c**)

Compound **5c** was synthesized according to a procedure that was similar to that of compound **5a**, except that compound **4c** was used in the place of compound **4a**. Orange solid; yield: 0.25 g (55%); m.p. 138–140°C; ^1H NMR (500 MHz, CDCl_3): $\delta=9.90$ (s, 1H), 7.99 (d, $J=8.0$ Hz, 1H), 7.91 (d, $J=8.5$ Hz, 1H), 7.73 (d, $J=4.0$ Hz, 1H), 7.59 (d, $J=1.0$ Hz, 1H), 7.49–7.54 (m, 4H), 7.28–7.29 (m, 2H), 7.23–7.26 (m, 4H), 6.98–7.12 (m, 13H), 4.15 (t, $J=7.0$ Hz, 3H), 1.80–1.84 (m, 3H), 1.74–1.77 (m, 2H), 1.29–1.32 (m, 2H), 0.86–0.90 (m, 4H), 0.38–0.41 ppm (m, 6H); ^{13}C NMR (125 MHz, CDCl_3): $\delta=182.7, 156.1, 151.4, 151.3, 148.3, 148.1, 147.5, 146.7, 146.62, 142.59, 141.8, 141.1, 137.6, 136.8, 136.6, 129.4, 129.2, 124.3, 124.0, 123.9, 123.7, 123.6, 122.4, 121.1, 120.2, 119.8, 119.60, 119.55, 117.8, 117.7, 116.8, 106.4, 103.8, 56.1, 42.7, 32.6, 31.2, 20.5, 13.8, 8.6$ ppm; IR (KBr): $\tilde{\nu}=1660\text{ cm}^{-1}$ (C=O); HRMS (ESI): m/z calcd for $\text{C}_{56}\text{H}_{49}\text{N}_3\text{OS}$: 811.3596 $[\text{M}+\text{H}]^+$; found: 811.3592.

5'-4-((7-(Diphenylamino)-9,9-diethyl-9H-fluoren-2-yl)(phenyl)amino)phenyl)-2,2'-bithiophene-5-carbaldehyde (**6a**)

Compound **6a** was prepared from the reaction between (5'-(1,3-dioxolan-2-yl)-2,2'-bithiophen-5-yl)tributylstannane and N^2 -(4-bromophenyl)-9,9-diethyl- N^2, N^7 -triphenyl-9H-fluorene-2,7-diamine (**4a**) according to the procedure described above for compound **5a**. The residue was purified by column chromatography on neutral alumina (hexanes/ CH_2Cl_2). Orange solid; yield: 0.206 g (50%); m.p. 140–142°C; ^1H NMR (500 MHz, CDCl_3): $\delta=10.00$ (d, $J=5.5$ Hz, 1H), 7.81–7.82 (m, 1H), 7.61–7.69 (m, 4H), 7.39–7.52 (m, 10H), 7.28–7.34 (m, 5H), 7.12–7.25 (m, 9H), 1.98–1.99 (m, 4H), 0.53–0.56 ppm (m, 6H); ^{13}C NMR (125 MHz, CDCl_3): $\delta=182.4, 154.5, 151.3, 148.2, 149.1, 147.6, 147.5, 147.2, 146.8, 146.4, 146.2, 146.0, 145.8, 141.3, 137.5, 137.4, 137.3, 136.4, 134.0, 132.1, 129.4, 129.2, 128.4, 127.3, 127.1, 126.9, 126.8, 126.6, 126.2, 124.8, 124.4, 124.3, 124.0, 123.9, 123.8, 123.7, 123.3, 123.2, 123.2, 123.1, 123.0, 122.8, 122.7, 122.4, 120.1, 119.9, 119.6, 119.5, 114.5, 56.2, 32.6, 8.6$ ppm; IR (KBr): $\tilde{\nu}=1659\text{ cm}^{-1}$ (C=O); HRMS (ESI): m/z calcd for $\text{C}_{50}\text{H}_{40}\text{N}_2\text{OS}_2$: 749.2655 $[\text{M}+\text{H}]^+$; found: 749.2655.

5'-7-((7-(Diphenylamino)-9,9-diethyl-9H-fluoren-2-yl)(phenyl)amino)-9,9-diethyl-9H-fluoren-2-yl)-2,2'-bithiophene-5-carbaldehyde (**6b**)

Compound **6b** was synthesized according to a procedure that was similar to that for compound **6a**, except that compound **4b** was used in the place of compound **4a**. Red-orange solid; yield: 0.32 g (65%); m.p. 190–192°C; ^1H NMR (500 MHz, CDCl_3): $\delta=9.87$ (d, $J=0.5$ Hz, 1H), 7.69 (dd, $J=4.0$ Hz, 0.5 Hz, 1H), 7.56–7.63 (m, 3H), 7.50–7.52 (m, 3H), 7.32–7.33 (m, 1H), 7.26–7.29 (m, 3H), 7.23–7.25 (m, 4H), 7.16 (d, $J=8.5$ Hz, 2H), 6.93–7.12 (m, 13H), 2.00 (dd, $J=14.0$ Hz, 7.0 Hz, 2H), 1.79–1.91 (m, 6H), 0.37–0.40 ppm (m, 12H); ^{13}C NMR (125 MHz, CDCl_3): $\delta=182.3, 159.0, 151.2, 150.5, 147.9, 146.4, 141.9, 141.3, 137.4, 136.5, 134.3, 131.2, 129.1, 127.0, 124.8, 123.7, 123.7, 122.4, 122.2, 119.8, 119.6, 119.4, 119.3, 119.0, 118.3, 56.2, 55.9, 32.6, 32.5, 8.50, 8.48$ ppm; IR (KBr): $\tilde{\nu}=1662\text{ cm}^{-1}$ (C=O); HRMS (ESI): m/z calcd for $\text{C}_{61}\text{H}_{52}\text{N}_2\text{OS}_2$: 893.3594 $[\text{M}+\text{H}]^+$; found: 893.3591.

5'-9-Butyl-7-((7-(diphenylamino)-9,9-diethyl-9H-fluoren-2-yl)(phenyl)amino)-9H-carbazol-2-yl)-2,2'-bithiophene-5-carbaldehyde (**6c**)

Compound **6c** was synthesized according to a procedure that was similar to that for compound **6a**, except that compound **4c** was used in the place of compound **4a**. Orange solid; yield: 0.17 g (35%); m.p. 108–110°C;

^1H NMR (500 MHz, CDCl_3): $\delta=9.87$ (s, 1H), 7.98 (d, $J=7.0$ Hz, 1H), 7.89–7.92 (m, 1H), 7.69 (d, $J=5.5$ Hz, 1H), 7.47–7.52 (m, 4H), 7.35–7.38 (m, 1H), 7.27–7.29 (m, 3H), 7.23–7.26 (m, 4H), 7.18 (d, $J=8.5$ Hz, 1H), 7.07–7.15 (m, 9H), 6.98–7.03 (m, 5H), 4.14–4.17 (m, 2H), 1.75–1.84 (m, 6H), 0.87–0.90 (m, 5H), 0.39–0.42 ppm (m, 6H); ^{13}C NMR (125 MHz, CDCl_3): $\delta=182.5, 151.3, 151.2, 148.4, 148.1, 147.8, 147.5, 147.1, 146.8, 146.6, 142.4, 141.3, 141.2, 137.5, 136.7, 136.6, 134.5, 130.0, 129.2, 127.3, 123.9, 123.8, 123.8, 123.7, 123.3, 122.9, 122.4, 120.9, 120.1, 119.8, 119.6, 119.5, 117.9, 117.5, 116.8, 105.7, 104.0, 56.1, 42.7, 32.6, 31.1, 20.5, 13.9, 8.6$ ppm; IR (KBr): $\tilde{\nu}=1660\text{ cm}^{-1}$ (C=O); HRMS (ESI): m/z calcd for $\text{C}_{60}\text{H}_{51}\text{N}_3\text{OS}_2$: 893.3474 $[\text{M}+\text{H}]^+$; found: 893.3439.

(E)-2-Cyano-3-(5-(4-((7-(diphenylamino)-9,9-diethyl-9H-fluoren-2-yl)(phenyl)amino)phenyl)thiophen-2-yl)acrylic acid (**7a**)

5-(4-((7-(diphenylamino)-9,9-diethyl-9H-fluoren-2-yl)(phenyl)amino)phenyl)thiophene-2-carbaldehyde (**5a**; 0.10 g, 0.15 mmol), cyanoacetic acid (0.019 g, 0.22 mmol), acetic acid (5 mL), and ammonium acetate (4 mg) were mixed together and heated at reflux for 12 h. The resulting red solution was poured into ice-cold water to produce an orange precipitate. This precipitate was filtered, washed thoroughly with water, and dried. The solid was further recrystallized with CHCl_3 . Red-brown solid; yield: 0.089 g (81%); m.p. 168–170°C; ^1H NMR (500 MHz, $[\text{D}_6]\text{DMSO}$): $\delta=8.43$ (s, 1H), 7.95 (d, $J=4.5$ Hz, 1H), 7.67–7.73 (m, 4H), 7.63 (d, $J=4.5$ Hz, 1H), 7.35–7.38 (m, 2H), 7.28–7.31 (m, 3H), 6.91–7.17 (m, 16H), 1.77–1.86 (m, 4H), 0.29 ppm (t, $J=7.0$ Hz, 6H); ^{13}C NMR (125 MHz, CDCl_3): $\delta=163.0, 156.2, 154.5, 151.4, 149.8, 148.0, 146.4, 145.6, 145.0, 140.5, 136.3, 134.2, 132.2, 130.4, 129.5, 129.4, 129.2, 127.8, 127.5, 125.0, 124.9, 124.1, 123.8, 122.5, 121.7, 120.4, 120.0, 119.5, 56.2, 32.6, 8.6$ ppm; IR (KBr): $\tilde{\nu}=2217\text{ cm}^{-1}$ (C≡N); HRMS (ESI): m/z calcd for $\text{C}_{49}\text{H}_{39}\text{N}_3\text{O}_2\text{S}$: 734.2836 $[\text{M}+\text{H}]^+$; found: 734.2846.

(E)-2-Cyano-3-(5-(7-((7-(diphenylamino)-9,9-diethyl-9H-fluoren-2-yl)(phenyl)amino)-9,9-diethyl-9H-fluoren-2-yl)thiophen-2-yl)acrylic acid (**7b**)

Compound **7b** was prepared from compound **5b** according to a procedure that was similar to that described above for compound **7a**. Red-brown solid; yield: 0.11 g (85%); m.p. 260–262°C; ^1H NMR (500 MHz, $[\text{D}_6]\text{DMSO}$): $\delta=8.48$ (s, 1H), 8.01 (d, $J=4.0$ Hz, 1H), 7.76–7.84 (m, 4H), 7.67 (dd, $J=8.0$ Hz, 3.0 Hz, 1H), 7.27–7.35 (m, 6H), 7.08–7.11 (m, 4H), 7.05–7.06 (m, 2H), 6.98–7.03 (m, 8H), 6.95 (dd, $J=8.5$ Hz, 2.0 Hz, 1H), 2.03–2.08 (m, 2H), 1.75–1.88 (m, 6H), 0.26–0.31 ppm (m, 6H); ^{13}C NMR (125 MHz, $[\text{D}_6]\text{DMSO}$): $\delta=163.6, 153.6, 121.3, 150.8, 150.7, 150.4, 147.7, 147.44, 147.37, 146.4, 146.1, 142.5, 141.3, 136.2, 136.1, 134.7, 134.2, 130.4, 129.5, 129.4, 125.7, 125.1, 124.9, 1123.6, 123.4, 123.1, 122.9, 122.6, 122.3, 121.4, 120.3, 120.2, 120.0, 116.2, 118.7, 117.6, 116.6, 55.8, 55.5, 31.8, 31.8, 8.5, 8.4$ ppm; IR (KBr): $\tilde{\nu}=2221\text{ cm}^{-1}$ (C≡N); HRMS (ESI): m/z calcd for $\text{C}_{60}\text{H}_{51}\text{N}_3\text{O}_2\text{S}$: 878.3775 $[\text{M}+\text{H}]^+$; found: 878.3779.

(E)-3-(5-(9-butyl-7-((7-(diphenylamino)-9,9-diethyl-9H-fluoren-2-yl)(phenyl)amino)-9H-carbazol-2-yl)thiophen-2-yl)-2-cyanoacrylic acid (**7c**)

Compound **7c** was prepared from compound **5c** according to a procedure that was similar to that described above for compound **7a**. Red solid; yield: 0.108 g (82%); m.p. 210–212°C; ^1H NMR (500 MHz, $[\text{D}_6]\text{DMSO}$): $\delta=8.49$ (s, 1H), 8.12 (d, $J=8.0$ Hz, 1H), 8.04–8.07 (m, 2H), 7.98 (s, 1H), 7.90 (d, $J=4.5$ Hz, 1H), 7.67 (dd, $J=8.5$ Hz, 5.0 Hz, 2H), 7.57 (dd, $J=8.0$ Hz, 1.5 Hz, 1H), 7.27–7.33 (m, 6H), 7.16 (d, $J=1.5$ Hz, 1H), 7.13 (d, $J=1.5$ Hz, 1H), 7.10 (d, $J=7.5$ Hz, 2H), 7.05–7.06 (m, 2H), 6.99–7.03 (m, 7H), 6.95 (dd, $J=8.0$ Hz, 2.0 Hz, 1H), 6.90 (dd, $J=8.5$ Hz, 1.5 Hz, 1H), 4.27 (t, $J=6.5$ Hz, 2H), 1.79 (dd, $J=14.5$ Hz, 7.0 Hz, 6H), 1.64 (t, $J=7.0$ Hz, 2H), 1.19 (dd, $J=15.0$ Hz, 7.5 Hz, 2H), 0.78 (t, $J=7.0$ Hz, 3H), 0.29–0.32 ppm (m, 6H); ^{13}C NMR (125 MHz, $[\text{D}_6]\text{DMSO}$): $\delta=163.7, 158.7, 154.5, 150.8, 150.8, 147.7, 147.4, 146.8, 146.4, 146.2, 146.0, 142.1, 141.2, 140.8, 136.2, 136.1, 134.0, 129.4, 128.8, 124.9, 123.8, 123.6, 123.4, 123.1, 122.7, 122.6, 121.5, 120.5, 120.3, 119.1, 117.7, 117.2, 116.7, 116.0, 106.5, 103.5, 55.5, 54.8, 38.9, 30.5, 19.6, 13.5, 8.4$ ppm; IR (KBr): $\tilde{\nu}=2217\text{ cm}^{-1}$

2216 cm⁻¹ (C≡N); HRMS (ESI): *m/z* calcd for C₅₉H₅₀N₄O₂S: 878.3654 [M+H]⁺; found: 878.3652.

(*E*)-2-Cyano-3-(5'-(4-((7-(diphenylamino)-9,9-diethyl-9H-fluoren-2-yl)(phenyl)amino)phenyl)-2,2'-bithiophen-5-yl)acrylic acid (**8a**)

Compound **8a** was prepared from compound **6a** according to a procedure that was similar to that described above for compound **7a**. Red-brown solid; 0.097 g (80 %); m.p. 226–228 °C; ¹H NMR (500 MHz, CDCl₃): δ = 8.47 (s, 1H), 7.96 (d, *J* = 4.0 Hz, 1H), 7.66–7.71 (m, 2H), 7.61–7.63 (m, 3H), 7.57 (d, *J* = 4.0 Hz, 1H), 7.49 (d, *J* = 3.5 Hz, 1H), 7.27–7.36 (m, 6H), 6.96–7.13 (m, 14H), 6.90–6.95 (m, 1H), 1.79–1.82 (m, 4H), 0.28–0.31 ppm (m, 6H); ¹³C NMR (125 MHz, CDCl₃): δ = 164.3, 157.2, 153.7, 152.5, 151.5, 147.7, 144.9, 143.7, 141.8, 140.4, 138.7, 136.9, 135.2, 133.9, 132.1, 129.3, 129.2, 128.1, 126.6, 124.8, 124.4, 124.0, 123.8, 122.7, 122.4, 120.2, 119.5, 56.1, 32.6, 8.6 ppm; IR (KBr): $\tilde{\nu}$ = 2217 cm⁻¹ (C≡N); HRMS (ESI): *m/z* calcd for C₅₃H₄₁N₃O₂S₂: 816.2713 [M+H]⁺; found: 816.2716.

(*E*)-2-Cyano-3-(5'-(7-((7-(diphenylamino)-9,9-diethyl-9H-fluoren-2-yl)(phenyl)amino)-9,9-diethyl-9H-fluoren-2-yl)-2,2'-bithiophen-5-yl)acrylic acid (**8b**)

Compound **8b** was prepared from compound **6b** according to a procedure that was similar to that described above for compound **7a**. Red solid; yield: 0.128 g (89 %); m.p. 209–211 °C; ¹H NMR (500 MHz, [D₆]DMSO): δ = 8.45 (s, 1H), 7.95 (d, *J* = 3.5 Hz, 1H), 7.77 (t, *J* = 8.0 Hz, 3H), 7.66–7.71 (m, 5H), 7.61 (d, *J* = 4.0 Hz, 1H), 7.27–7.34 (m, 6H), 6.97–7.09 (m, 14H), 6.95 (dd, *J* = 8.0 Hz, 1.5 Hz, 1H), 2.03–2.08 (m, 2H), 1.75–1.87 (m, 6H), 0.26–0.31 ppm (m, 12H); ¹³C NMR (125 MHz, [D₆]DMSO): δ = 156.4, 154.2, 151.1, 150.8, 150.7, 150.3, 147.4, 147.3, 146.2, 146.0, 145.3, 141.2, 141.0, 136.2, 136.0, 135.1, 133.9, 133.6, 130.9, 129.5, 129.4, 128.2, 125.1, 124.7, 123.7, 123.5, 123.1, 122.8, 122.5, 121.1, 120.3, 119.6, 119.2, 118.6, 117.9, 116.8, 55.8, 55.5, 31.8, 31.8, 8.5, 8.4 ppm; IR (KBr): $\tilde{\nu}$ = 2212 cm⁻¹ (C≡N); HRMS (ESI): *m/z* calcd for C₆₄H₅₃N₃O₂S₂: 960.3652 [M+H]⁺; found: 960.3658.

(*E*)-3-(5'-(9-Butyl-7-((7-(diphenylamino)-9,9-diethyl-9H-fluoren-2-yl)(phenyl)amino)-9H-carbazol-2-yl)-2,2'-bithiophen-5-yl)-2-cyanoacrylic acid (**8c**)

Compound **8c** was prepared from compound **6c** according to a procedure that was similar to that described above for compound **7a**. Red-brown solid; yield: 0.115 g (80 %); m.p. 240–243 °C; ¹H NMR (500 MHz, [D₆]DMSO): δ = 8.47 (s, 1H), 8.03 (dd, *J* = 16.0 Hz, 8.0 Hz, 2H), 7.96 (d, *J* = 4.0 Hz, 1H), 7.88 (s, 1H), 7.72 (d, *J* = 3.5 Hz, 1H), 7.60–7.69 (m, 4H), 7.51 (d, *J* = 9.0 Hz, 1H), 7.26–7.31 (m, 6H), 7.13 (d, *J* = 11.0 Hz, 2H), 7.07 (d, *J* = 8.0 Hz, 2H), 6.99–7.04 (m, 6H), 6.92–6.94 (m, 1H), 6.80 (d, *J* = 9.0 Hz, 1H), 4.25 (s, 2H), 1.76 (d, *J* = 7.0 Hz, 4H), 1.62 (s, 2H), 1.18 (d, *J* = 8.0 Hz, 2H), 0.76 (t, *J* = 7.0 Hz, 3H), 0.30 ppm (t, *J* = 7.0 Hz, 6H); ¹³C NMR (125.77 MHz, [D₆]DMSO): δ = 163.6, 150.8, 150.8, 147.8, 147.4, 146.9, 146.3, 146.0, 141.9, 140.9, 136.2, 136.1, 133.8, 133.5, 129.5, 129.4, 128.3, 123.7, 123.2, 123.1, 122.5, 121.3, 119.2, 119.0, 117.5, 117.1, 116.1, 103.9, 55.5, 41.7, 31.7, 30.6, 19.7, 13.6, 8.4 ppm; IR (KBr): $\tilde{\nu}$ = 2217 cm⁻¹ (C≡N); HRMS (ESI): *m/z* calcd for C₆₃H₅₂N₄O₂S₂: 960.3532 [M+H]⁺; found: 960.3500.

Computational Methods

All of the computations were performed with the Gaussian 09^[33] program package on a computer workstation. The ground-state geometries were fully optimized without any symmetry constraints at the DFT level with Becke's three-parameter hybrid functional and Lee, Yang, and Parr's correlation functional (B3LYP) by using the 6-31G** basis set on all atoms.^[31,32] The default parameters were used for the convergence criteria. Vibrational analysis was performed to confirm the optimized structures. The excitation energies and oscillator strengths for the lowest ten singlet transitions at the optimized geometry in the ground state were obtained by TD-DFT calculations by using the same basis set as for the geometry minimization.

Fabrication and Characterization of the DSSCs

The DSSCs were fabricated and characterized according to procedures that we have reported previously.^[13] The dye-sensitized photoanodes were formed by immersing the TiO₂-coated ITO plates (about 15 μ m thickness and 20 nm particle size TiO₂ layer/4 μ m scattering TiO₂ layer) in solutions of the dyes in a mixed-solvent system (MeCN/*t*-BuOH/DMSO, 3.5:3.5:3 v/v). The electrolyte was composed of 0.1 M LiI, 0.6 M 1-propyl-2,3-dimethylimidazolium iodide (DMPII), 0.05 M I₂, and 0.5 M *tert*-butylpyridine (TBP) in MeCN/3-methoxypropionitrile (MPN, 1:1 v/v). The absorption spectra of the dye-coated TiO₂ films were obtained on a UV/Vis spectrophotometer (JASCO) that was equipped with an integrating sphere accessory. The baseline was corrected by using a bare-TiO₂-coated FTO substrate.

Acknowledgements

K.R.J.T. is thankful to the Department of Science and Technology, New Delhi, India, for financial support (Ref. No. DST/TSG/ME/2010/27). K.-C.H. acknowledges a grant-in-aid from the National Science Council, Taiwan. A.B. acknowledges a Senior Research Fellowship from the CSIR, New Delhi.

- a) A. Hagfeldt, G. Boschloo, L. Sun, L. Kloo, H. Pettersson, *Chem. Rev.* **2010**, *110*, 6595–6663; b) Y. Ooyama, Y. Harima, *Eur. J. Org. Chem.* **2009**, 2903–2934; c) Z. Ning, H. Tian, *Chem. Commun.* **2009**, 5483–5495.
- a) I. Stengel, N. Pootrakulchote, R. R. Dykeman, A. Mishra, S. M. Zakeeruddin, P. J. Dyson, M. Grätzel, P. Bäuerle, *Adv. Energy Mater.* **2012**, *2*, 1004–1012; b) C.-Y. Chen, N. Pootrakulchote, T.-H. Hung, C.-J. Tan, H.-H. Tsai, S. M. Zakeeruddin, C.-G. Wu, M. Grätzel, *J. Phys. Chem. C* **2011**, *115*, 20043–20050; c) S. M. Feldt, E. A. Gibson, E. Gabrielsson, L. Sun, G. Boschloo, A. Hagfeldt, *J. Am. Chem. Soc.* **2010**, *132*, 16714–16724; d) A. Reynal, E. Palomares, *Eur. J. Inorg. Chem.* **2011**, 4509–4526; e) J.-G. Chen, S.-J. Wu, J.-Y. Li, C.-G. Wu, K.-C. Ho, *Angew. Chem.* **2008**, *120*, 7452–7455; *Angew. Chem. Int. Ed.* **2008**, *47*, 7342–7345.
- C.-J. Yang, Y. J. Chang, M. Watanabe, Y.-S. Hon, T. J. Chow, *J. Mater. Chem.* **2012**, *22*, 4040–4049.
- a) S. Jungsuttiwong, R. Tarsang, S. Pansay, T. Yakhantip, V. Promarak, T. Sudyoasuk, T. Kaewin, S. Saengsuwan, S. Namuangrak, *World Academy of Science Engineering and Technology* **2011**, *77*, 561–567; b) J. Tang, J. Hua, W. Wu, J. Li, Z. Jin, Y. Long, H. Tian, *Energy Environ. Sci.* **2010**, *3*, 1736–1745; c) Z. Ning, Q. Zhang, W. Wu, H. Pei, B. Liu, H. Tian, *J. Org. Chem.* **2008**, *73*, 3791–3797.
- a) Y. Wu, X. Zhang, W. Li, Z.-S. Wang, H. Tian, W. Zhu, *Adv. Energy Mater.* **2012**, *2*, 149–156; b) K. Pei, Y. Wu, W. Wu, Q. Zhang, B. Chen, H. Tian, W. Zhu, *Chem. Eur. J.* **2012**, *18*, 8190–8200; c) Y. Cui, Y. Wu, X. Lu, X. Zhang, G. Zhou, F. B. Miaph, W. Zhu, Z.-S. Wang, *Chem. Mater.* **2011**, *23*, 4394–4401; d) W. Zhu, Y. Wu, S. Wang, W. Li, X. Li, J. Chen, Z.-S. Wang, H. Tian, *Adv. Funct. Mater.* **2011**, *21*, 756–763.
- a) H. Han, M. Liang, K. Tang, X. Cheng, X. Zong, Z. Sun, S. Xue, *J. Photochem. Photobiol. A* **2011**, *225*, 8–16; b) N. Koumura, Z.-S. Wang, S. Mori, M. Miyashita, E. Suzuki, K. Hara, *J. Am. Chem. Soc.* **2006**, *128*, 14256–14257.
- a) J. N. Clifford, E. Martínez-Ferrero, A. Viterisi, E. Palomares, *Chem. Soc. Rev.* **2011**, *40*, 1635–1646; b) T. W. Hamann, R. A. Jensen, A. B. F. Martinson, H. Van Ryswyk, J. T. Hupp, *Energy Environ. Sci.* **2008**, *1*, 66–78.
- a) J. L. Segura, H. Herrera, P. Bäuerle, *J. Mater. Chem.* **2012**, *22*, 8717–8733; b) D. Kumar, K. R. J. Thomas, C.-P. Lee, K.-C. Ho, *Org. Lett.* **2011**, *13*, 2622–2625; c) X.-H. Zhang, Y. Cui, R. Katoh, N. Koumura, K. Hara, *J. Phys. Chem. C* **2010**, *114*, 18283–18290; d) M. K. R. Fischer, S. Wenger, M. Wang, A. Mishra, S. M. Zakeeruddin, M. Grätzel, P. Bäuerle, *Chem. Mater.* **2010**, *22*, 1836–1845.

- [9] a) Z.-M. Tang, T. Lei, K.-J. Jiang, Y.-L. Song, J. Pei, *Chem. Asian J.* **2010**, *5*, 1911–1917; b) M. Velusamy, K. R. J. Thomas, J. T. Lin, Y.-C. Hsu, K.-C. Ho, *Org. Lett.* **2005**, *7*, 1899–1902.
- [10] a) J. Mao, F. Guo, W. Ying, W. Wu, J. Li, J. Hua, *Chem. Asian J.* **2012**, *7*, 982–991; b) W. Li, Y. Wu, Q. Zhang, H. Tian, W. Zhu, *ACS Appl. Mater. Interfaces* **2012**, *4*, 1822–1830.
- [11] a) C.-H. Chen, Y.-C. Hsu, H.-H. Chou, K. R. J. Thomas, J. T. Lin, C.-P. Hsu, *Chem. Eur. J.* **2010**, *16*, 3184–3193; b) H. Choi, C. Baik, S. O. Kang, J. Ko, M.-S. Kang, M. K. Nazeeruddin, M. Grätzel, *Angew. Chem.* **2008**, *120*, 333–336; *Angew. Chem. Int. Ed.* **2008**, *47*, 327–330; c) J.-J. Kim, H. Choi, J.-W. Lee, M.-S. Kang, K. Song, S. O. Kang, J. Ko, *J. Mater. Chem.* **2008**, *18*, 5223–5229; d) M. Wang, M. Xu, D. Shi, R. Li, F. Gao, G. Zhang, Z. Yi, R. Humphry-Baker, P. Wang, S. M. Zakeeruddin, M. Grätzel, *Adv. Mater.* **2008**, *20*, 4460–4463; e) H. Choi, J. K. Lee, K. Song, S. O. Kang, J. Ko, *Tetrahedron* **2007**, *63*, 3115–3121; f) I. Jung, J. K. Lee, K. H. Song, K. Song, S. O. Kang, J. Ko, *J. Org. Chem.* **2007**, *72*, 3652–3658; g) S. Kim, J. K. Lee, S. O. Kang, J. Ko, J.-H. Yum, S. Fantacci, F. D. Angelis, D. D. Censo, M. K. Nazeeruddin, M. Grätzel, *J. Am. Chem. Soc.* **2006**, *128*, 16701–16707.
- [12] a) L.-Y. Lin, C.-H. Tsai, K.-T. Wong, T.-W. Huang, L. Hsieh, S.-H. Liu, H.-W. Lin, C.-C. Wu, S.-H. Chou, S.-H. Chen, A.-I. Tsai, *J. Org. Chem.* **2010**, *75*, 4778–4785; b) D. P. Hagberg, X. Jiang, E. Gabrielson, M. Linder, T. Marinado, T. Brinck, A. Hagfeldt, L. Sun, *J. Mater. Chem.* **2009**, *19*, 7232–7238.
- [13] a) A. Baheti, P. Singh, C.-P. Lee, K. R. J. Thomas, K.-C. Ho, *J. Org. Chem.* **2011**, *76*, 4910–4920; b) K. R. J. Thomas, N. Kapoor, C.-P. Lee, K.-C. Ho, *Chem. Asian J.* **2012**, *7*, 738–750.
- [14] S. Haid, M. Marszalek, A. Mishra, M. Wielopolski, J. Teuscher, J.-E. Moser, R. Humphry-Baker, S. M. Zakeeruddin, M. Grätzel, P. Bäuerle, *Adv. Funct. Mater.* **2012**, *22*, 1291–1302.
- [15] a) S. Gong, Y. Zhao, C. Yang, C. Zhong, J. Qin, D. Ma, *J. Phys. Chem. C* **2010**, *114*, 5193–5198; b) Z. Zhao, X. Xu, H. Wang, P. Lu, G. Yu, Y. Liu, *J. Org. Chem.* **2008**, *73*, 594–602; c) J. Li, D. Liu, Y. Li, C.-S. Lee, H.-L. Kwong, S. Lee, *Chem. Mater.* **2005**, *17*, 1208–1212.
- [16] P. J. Low, M. A. J. Paterson, D. S. Yufit, J. A. K. Howard, J. C. Cherrym, D. R. Tackley, R. Brookc, B. Brown, *J. Mater. Chem.* **2005**, *15*, 2304–2315.
- [17] J. F. Hartwig, *Angew. Chem.* **1998**, *110*, 2154–2177; *Angew. Chem. Int. Ed.* **1998**, *37*, 2046–2067.
- [18] J. K. Stille, *Angew. Chem.* **1986**, *98*, 504–519; *Angew. Chem. Int. Ed. Engl.* **1986**, *25*, 508–524.
- [19] E. Knoevenagel, *Chem. Ber.* **1896**, *29*, 172–174.
- [20] a) A. Mishra, N. Pootrakulchote, M. Wang, S.-J. Moon, S. M. Zakeeruddin, M. Grätzel, P. Bäuerle, *Adv. Funct. Mater.* **2011**, *21*, 963–970; b) A. Mishra, M. K. R. Fischer, P. Bäuerle, *Angew. Chem.* **2009**, *121*, 2510–2536; *Angew. Chem. Int. Ed.* **2009**, *48*, 2474–2499.
- [21] M. K. Nazeeruddin, A. Kay, I. Rodicio, R. Humphrey-Baker, E. Müller, P. Liska, N. Vlachopoulos, M. Grätzel, *J. Am. Chem. Soc.* **1993**, *115*, 6382–6390.
- [22] a) C. Pérez León, L. Kador, B. Peng, M. Thelakkat, *J. Phys. Chem. B* **2005**, *109*, 5783–5789; b) M. K. Nazeeruddin, R. Humphry-Baker, P. Liska, M. Grätzel, *J. Phys. Chem. B* **2003**, *107*, 8981–8987.
- [23] a) Y. Ooyama, S. Inoue, T. Nagano, K. Kushimoto, J. Ohshita, I. Imae, K. Komaguchi, Y. Harima, *Angew. Chem.* **2011**, *123*, 7567–7571; *Angew. Chem. Int. Ed.* **2011**, *50*, 7429–7433; b) T. Leijtens, I.-K. Ding, T. Giovenzana, J. T. Bloking, M. D. McGehee, A. Sellinger, *ACS Nano* **2012**, *6*, 1455–1462.
- [24] a) A. Granzhan, H. Ihmels, G. Viola, *J. Am. Chem. Soc.* **2007**, *129*, 1254–1267; b) O. van den Berg, W. F. Jager, S. J. Picken, *J. Org. Chem.* **2006**, *71*, 2666–2676.
- [25] a) Q. Feng, X. Lu, G. Zhou, Z.-S. Wang, *Phys. Chem. Chem. Phys.* **2012**, *14*, 7993–7999; b) E. Miyazaki, T. Okanishi, Y. Suzuki, N. Ishine, H. Mori, K. Takimiya, Y. Harima, *Bull. Chem. Soc. Jpn.* **2011**, *84*, 459–465; c) A. Baheti, P. Tyagi, K. R. J. Thomas, Y.-C. Hsu, J. T. Lin, *J. Phys. Chem. C* **2009**, *113*, 8541–8547; d) K. R. Justin Thomas, Y.-C. Hsu, J. T. Lin, K.-M. Lee, K.-C. Ho, C.-H. Lai, Y.-M. Cheng, P.-T. Chou, *Chem. Mater.* **2008**, *20*, 1830–1840.
- [26] D. P. Hagberg, T. Marinado, K. M. Karlsson, K. Nonomura, P. Qin, G. Boschloo, T. Brinck, A. Hagfeldt, L. Sun, *J. Org. Chem.* **2007**, *72*, 9550–9556.
- [27] Y. J. Chang, T. J. Chow, *Tetrahedron* **2009**, *65*, 4726–4734.
- [28] a) R. Potyrailo, K. Rajan, K. Stoewe, I. Takeuchi, B. Chisholm, H. Lam, *ACS Comb. Sci.* **2011**, *13*, 579–633; b) K. Rurack, J. L. Bricks, G. Reck, R. Radeaglia, U. Resch-Genger, *J. Phys. Chem. A* **2000**, *104*, 3087–3109; c) J. A. Pollard, D. Zhang, J. A. Downing, F. J. Knorr, J. L. McHale, *J. Phys. Chem. A* **2005**, *109*, 11443–11452.
- [29] C. M. Elliott, *Nat. Chem.* **2011**, *3*, 188–189.
- [30] M. Grätzel, *Nature* **2001**, *414*, 338–344.
- [31] R. G. Parr, W. T. Yang, *Annu. Rev. Phys. Chem.* **1995**, *46*, 701–728.
- [32] a) A. D. Becke, *J. Chem. Phys.* **1993**, *98*, 1372–1377; b) C. Lee, W. Yang, R. G. Parr, *Phys. Rev. B* **1988**, *37*, 785–789.
- [33] Gaussian 09, Revision A.02, M. J. Frisch, G. W. Trucks, H. B. Schlegel, G. E. Scuseria, M. A. Robb, J. R. Cheeseman, G. Scalmani, V. Barone, B. Mennucci, G. A. Petersson, H. Nakatsuji, M. Caricato, X. Li, H. P. Hratchian, A. F. Izmaylov, J. Bloino, G. Zheng, J. L. Sonnenberg, M. Hada, M. Ehara, K. Toyota, R. Fukuda, J. Hasegawa, M. Ishida, T. Nakajima, Y. Honda, O. Kitao, H. Nakai, T. Vreven, J. A., Jr., Montgomery, J. E. Peralta, F. Ogliaro, M. Bearpark, J. J. Heyd, E. Brothers, K. N. Kudin, V. N. Staroverov, R. Kobayashi, J. Normand, K. Raghavachari, A. Rendell, J. C. Burant, S. S. Iyengar, J. Tomasi, M. Cossi, N. Rega, N. J. Millam, M. Klene, J. E. Knox, J. B. Cross, V. Bakken, C. Adamo, J. Jaramillo, R. Gomperts, R. E. Stratmann, O. Yazyev, A. J. Austin, R. Cammi, C. Pomelli, J. W. Ochterski, R. L. Martin, K. Morokuma, V. G. Zakrzewski, G. A. Voth, P. Salvador, J. J. Dannenberg, S. Dapprich, A. D. Daniels, Ö Farkas, J. B. Foresman, J. V. Ortiz, J. Cioslowski, D. J. Fox, Gaussian, Inc., Wallingford, CT, **2009**.
- [34] B. J. Lynch, P. L. Fast, M. Harris, D. G. Truhlar, *J. Phys. Chem. A* **2000**, *104*, 4811–4815.
- [35] S.-Q. Fana, Y. Geng, C. Kima, S. Paika, J. Ko, *Mater. Chem. Phys.* **2012**, *132*, 943–949.
- [36] B. Wenger, M. Grätzel, J.-E. Moser, *J. Am. Chem. Soc.* **2005**, *127*, 12150–12151.
- [37] D. Kuang, S. Uchida, R. Humphry-Baker, S. M. Zakeeruddin, M. Grätzel, *Angew. Chem.* **2008**, *120*, 1949–1953; *Angew. Chem. Int. Ed.* **2008**, *47*, 1923–1927.
- [38] a) I. Mora-Seró, S. Giménez, F. Fabregat-Santiago, R. Gómez, Q. Shen, T. Toyoda, J. Bisquert, *Acc. Chem. Res.* **2009**, *41*, 1848–1857; b) J. van de Lagemaat, N.-G. Park, A. J. Frank, *J. Phys. Chem. B* **2000**, *104*, 2044–2052.

Received: August 16, 2012

Published online: September 28, 2012